Development of a Novel SERS Assay for the Detection of MiRNA and the Synthesis and Use of Lipid Soluble Nanoparticles for the Application to Cardiovascular Disease

by

Millie Kennedy-Goor

Jan 2018

Development of a Novel SERS Assay for the Detection of MiRNA and Synthesis and Use of Lipid Soluble Nanoparticles for the Application to Cardiovascular Disease

by

Millie Kennedy-Goor

A thesis submitted to the Department of Pure and Applied Chemistry, University of Strathclyde, in part fulfilment of the regulations for the degree of Master of Philosophy

I certify that the thesis has been written by me. Any help I have received in my research work and the preparation of the thesis itself has been acknowledged. In addition, I certify that all information sources and literature used are indicated in the thesis.

Signed:  **Jan 2018**

Acknowledgements

I would like to express my extreme gratitude to Professor Duncan Graham for all his support during this project. It has been a tough and prolonged journey for which I am eternally grateful to have had the opportunity to take.

I would like to thank Isobel Scott and Professor Christine Davidson for helping in the organisation and submission of this project.

Abstract

Cardiovascular disease (CVD) encompasses a wide range of clinical conditions including atherosclerosis. This progressive inflammatory disease can develop and present no symptoms for a long period of time before classifying as clinical. Current detection methods include the non-invasive technique of x-rays and the invasive technique of angiography. Both of these have several limitations including the delayed timeframe from which they can detect the disease. It is desirable for a technique to be able to detect early (sub-clinical) stages, to allow early treatment and the best possible chances patient recovery.

Small endogenous RNA species (microRNA's) play an important role in cardiac homeostasis, therefore lending themselves as potential biomarkers. This research demonstrates the use of nanoparticle-oligonucleotide conjugates, together with surface-enhanced Raman scattering (SERS) to detect and identify CVD specific microRNA sequences. The use of a Raman reporter functionalised to the nanoparticle surface allows a signal to be obtained and thus an attribute by which the presence, or lack of, a target microRNA sequence can be concluded.

In order for such species to be used for clinical purposes, they must be capable of passing through the cell membrane. This research shows the synthesis of cholesterol covered particles and their ability to penetrate the phospholipid bilayer, thus demonstrating their potential to act as a biomarker detector.

Contents

List of Figures

List of Tables

List of Equations

1. Introduction

1.1. Raman Spectroscopy

Spectroscopy is the study of the way in which light interacts with molecules in order to gain information on the molecular structure of a sample. Spectroscopic techniques exploit at least one of three optical processes; absorption, emission or scattering. For the case of Raman spectroscopy, we are concerned with the scattering of light from a sample.

For a molecule to be Raman active, it must be polarisable. Raman is often referred to as a complementary technique to IR spectroscopy which requires a induced dipole [1]. When a Raman active molecule is excited by a photon, the interaction between the photon and the molecule causes a distortion in the electron cloud resulting in an induced dipole. It is for this reason that a Raman active molecule must be polarisable. When the molecule possesses this induced dipole, it is said to be in the 'excited' state, however, this state is not a true state of the molecule. It is referred to as a 'virtual' state that lasts only a transient amount of time before returning to the relaxed, electronic ground state [2]. During this relaxation process scattering of light occurs. This can be represented using energy level diagrams as shown in Figure 1.1. Note that in the energy level diagrams, the virtual energy state is represented by a dashed line and not a solid line to indicate that it is not a permanent energy level. It is this scattering process that is measured and exploited by Raman spectroscopy in order to gain structural information about the sample being analysed. Also note, that in the energy level diagrams, the electron transfers are represented by a straight line. This is to symbolise the fact that electrons move at an infinitely fast speed in comparison to the nuclei of an atom according to the Frank-Condon principle [3].

During the scattering process, there are three possible outcomes. The scattered light may have the same frequency as the incident light and therefore return to the initial ground state energy level. In this case, the difference in energy between the incident and scattered light is zero and thus the molecule will possess the same quanta of energy after scattering as it did pre-excitation. This is known as Rayleigh scattering (also known as elastic scattering). Rayleigh scattering accounts for the majority of scattered light.

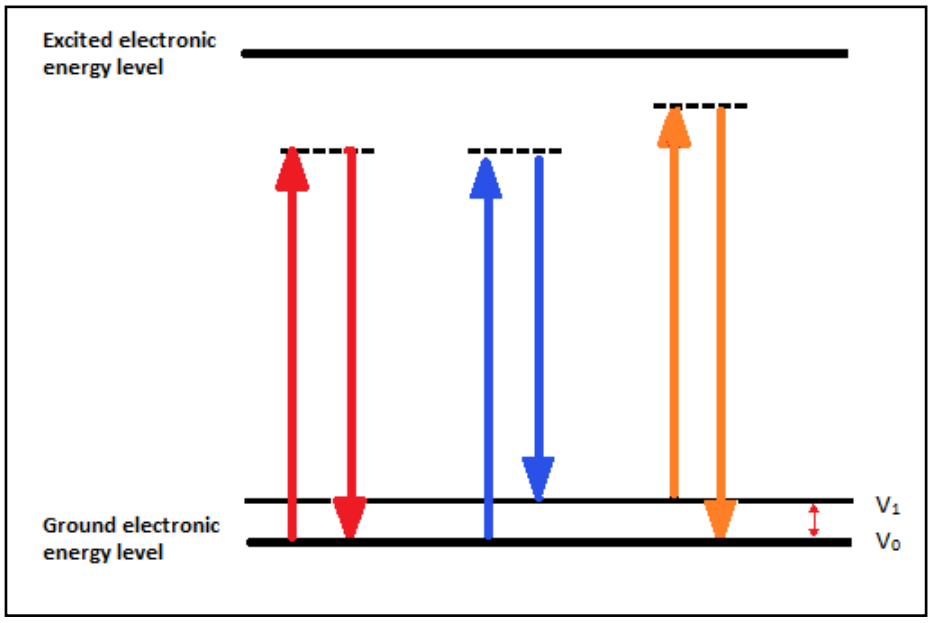

Figure 1.1. Schematic displaying the different types of scattering. Rayleigh scattering is displayed in red with no change in energy. Stokes Raman scattering is displayed in blue and anti-Stokes in orange, both with a change in energy. The change in energy is equal to the energy difference between the ground vibrational energy level and the first excited vibrational energy level ($\Delta V=\pm 1$) within the ground electronic state.

However, a small proportion of molecules experience inelastic scattering, also known as Raman scattering, whereby there is an energy difference between the incident and scattered light. If the electron returns to the ground electronic state yet a higher vibrational energy level state, this is known as Stokes scattering and consequently there is positive difference in the energy ratio between the incident and scattered light. In a few cases, a molecule may exist in an excited vibrational state within the ground electronic state. During relaxation following excitation, it returns to a lower vibrational energy level within the ground electronic state. In this case, there is a negative difference in energy between the incident and scattered light. This is known as anti-Stokes scattering. As described by the Boltzmann distribution there is a much higher proportion of molecules at room temperature lying in the ground vibrational state compared to an excited vibrational state and consequently, anti-Stokes scattering is less likely to occur and hence the response is much weaker than Stokes scattering [2]. It is for this reason that Stokes scattering is most often measured in Raman spectroscopy.

The Raman scattering of a sample is represented by the shift in energy from the incident laser frequency. This is called the Raman shift and has units of cm^{-1}. As it is Stokes scattering that is measured, the scattered light possesses less energy than the incident light thus the energy change and consequently Raman shifts have positive values.

Although Raman spectroscopy is an important spectroscopic technique, there are two major drawbacks.

Firstly, Raman spectroscopy is highly insensitive. It is estimated that around only one in 10^7 scattered photons are Raman scattered and thus the intensity of the signal in comparison to Rayleigh scattering is extremely weak. The intensity of Raman scattering has a fourth power dependence on the frequency of the incident light as demonstrated by Equations 1 and 2 [2, 4]. Since the frequency of light is related to the wavelength of light, the choice of wavelength of the incident light is of extreme importance. As the wavelength of light decreases, the scattering intensity increases. However, at lower frequencies, fluorescence becomes more of an issue, therefore a compromise must be reached in order to gain the optimum wavelength that produces high scattering intensity with the lowest fluorescence interference.

$$I = KI_L\alpha^2\nu^4 \qquad I_s = \frac{1}{\lambda^4} \qquad (1,2)$$

Equation 1. Displaying the fourth power dependence of scattering intensity on frequency, where I = intensity, K = constant, I_L = laser power, α = polarizability of electrons in the molecule and ν = frequency of incident radiation.

The other drawback of Raman spectroscopy as just mentioned is fluorescence. Fluorescence, like Raman scattering is an optical process. It occurs when a fluorescent material absorbs light which results in the excitation of an electron followed by a relaxation process [5]. During the relaxation process, emission of light occurs. The emitted radiation may have the same (resonance), a longer or a shorter wavelength than the incident radiation. The highest intensity emitted light possesses a longer wavelength hence lower energy than the incident light. Like with Raman scattering, Fluorescence can be represented using an energy level diagram as shown in Figure 1.2.

Fluorescence is an extremely strong process and due to this is much more intense than Raman scattering. As a consequence, fluorescence often interferes with the detection of Raman scattering. It displays itself as background interference on a Raman spectrum and due to its much higher intensity often masks peaks, thus making it extremely difficult to accurately and reliably measure the Raman scattering of a sample in the presence of fluorescence.

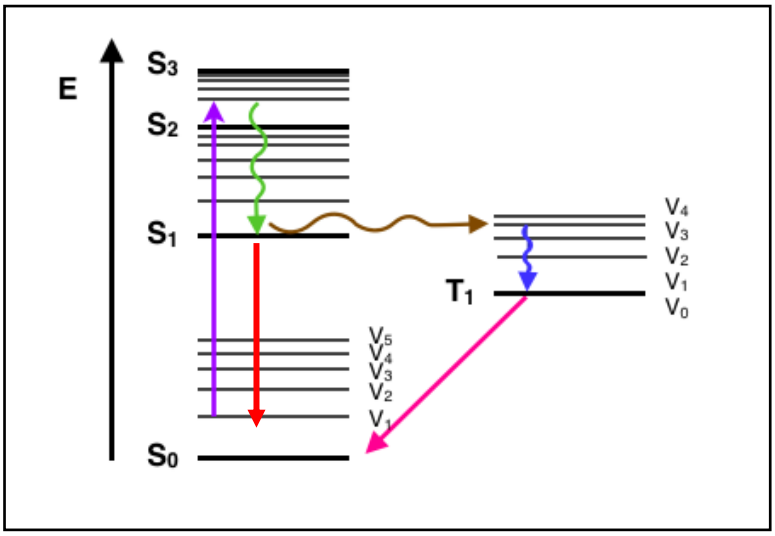

Figure 1.2. Jablonski diagram adapted from [6]. Horizontal lines represent different energy levels with each bold line representing an electronic energy level and the thinner lines representing vibrational energy levels. S_X and T_X represent singlet and triplet spin states respectively. Downwards vertical arrows show the occurrence of fluorescence (within the same spin state) and phosphorescence (between spin states). Curly lines display the occurrence of relaxation or intersystem crossing. Fluorescence is displayed by the red downwards arrow.

Over the past few decades, a vast amount of research has been carried out on Raman spectroscopy with the aim to enhance its sensitivity and quench the effects of fluorescence in order to present Raman spectroscopy as an efficient and effective analytical technique. This has subsequently led to the evolution of a number of enhancement techniques such as tip-enhancement Raman scattering (TERS) and of greatest importance to this work, surface enhanced Raman scattering (SERS) and surface enhanced resonance Raman scattering (SERRS) [7-9].

1.1.1. Surface Enhanced Raman Spectroscopy (SERS)

In 1974, experimentation using roughened silver electrodes as a surface upon which the Raman scattering of pyridine was being detected enabled the discovery of the now well used technique surface-enhanced Raman scattering (SERS) [10]. Their aim was to study the behaviour of species adsorbed onto electrodes using Raman spectroscopy. They decided to use electrodes with high surface areas to maximise possible adsorption and study possible behaviours exhibited.

They saw an incomprehensible increase in the scattering intensities of pyridine when absorbed onto a roughened silver electrode compared to liquid pyridine. As stated by one of the researchers involved in this discovery, A. J. McQuillan, the intensity increase of Raman scattering of a species using high surface area metals is about 10^6. It has even been reported to increase scattering

intensity by 10^{14} [11]. It is this metal surface enhancement of Raman scattering that will be exploited in this project by the use of silver nanoparticles.

In 1977, following further studies showing the enhancement of Raman scattering of species adsorbed on a roughened metal surface, it was proposed that the enhancement effect is due to a combination of two mechanisms; the electromagnetic effect and the chemical effect [12].

1.1.1.1. Electromagnetic Enhancement

This effect relies on the fact that certain metal surfaces such as gold, silver, aluminium and copper are surrounded by coupled photons and electrons also known as plasmons [13]. These metals are known as quasi-free electron metals.

There are two forms of plasmon resonance; propagated plasmon resonance and localised plasmon resonance. The former resonance is present on elongated surfaces, whilst more importantly to this project, the latter is present on the surface of a spherical particle [8]. Upon excitation of this surface plasmon via the incident laser light, the local electric field experienced by the molecule is greatly enhanced. This field enhancement influences the incident laser field, as well as the scattered light field which in turn amplifies the overall intensity of the Raman scattered light [14].

The total Raman signal enhancement is proportional to E^4. Thus for a small deviation in the local field, a large increase in scattering intensity can be observed.

This electromagnetic effect is considered to be the dominant mechanism in the enhancement of Raman scattering intensity in SERS [14].

1.1.1.2. Chemical Enhancement

Campion and Kambhampati also demonstrated how SERS may be a consequence of a chemical enhancement process [8]. They proposed two explanations.

The first being that the electronic states of the adsorbed analyte are broadened due to their interaction with the surface and the second being when the analyte is adsorbed onto the surface, new electronic energy states are present which act as resonant intermediate states in Raman scattering.

Both of these would result in the highest occupied molecular orbital (HOMO) and the lowest unoccupied molecular orbital (LUMO) of the analyte being symmetrically disposed with the Fermi-level of the metal which in turn allows for excitation to occur at half the original energy of the adsorbate.

Although the chemical enhancement explanations provided by Campion and Kambhampati offer a reasonable elucidation for the SERS effect, many scientists are hesitant and believe the electromagnetic effect is the main, if not the only process causing the SERS effect.

1.2. Cardiovascular Disease

Cardiovascular disease (CVD) is an encapsulating term used to define any disease relating to the cardiac or vascular system. This encompasses a broad range of medical conditions from minor angina to coronary heart disease to possibly fatal heart failure and stroke.

As the leading cause of death in the USA [15] and a cause of a quarter of all deaths in the UK [16] according to the American Heart Association and British Heart Foundation respectively, CVD is an area of high interest in clinical research. Yet despite major advances in both diagnostics and therapeutics for CVD, it remains the world's biggest killer (except Africa) [17]. Thus more research is required to improve on existing techniques and develop new methods for identifying and treating CVD's. One area of particular interest is that of nanomedicine which has shown promising potential.

The specific causes of CVD depend on the affecting disease. However, most CVD's are a consequence of a disruption in blood flow around the body. This is primarily caused by a progressive process known as atherosclerosis which gradually narrows the passageway for blood due to a build up of fatty plaques.

1.2.1. Atherosclerosis Development

Atherosclerosis can be described as a 'chronic, progressive inflammatory disease' [18]. The gradual process may take the course of decades before any symptoms are presented. Prior to symptoms, such a stage would be classed as subclinical; asymptomatic. When symptoms present themselves, it becomes known as the clinical stage. A cross sectional schematic showing the progression of atherosclerosis is shown in Figure 1.3.

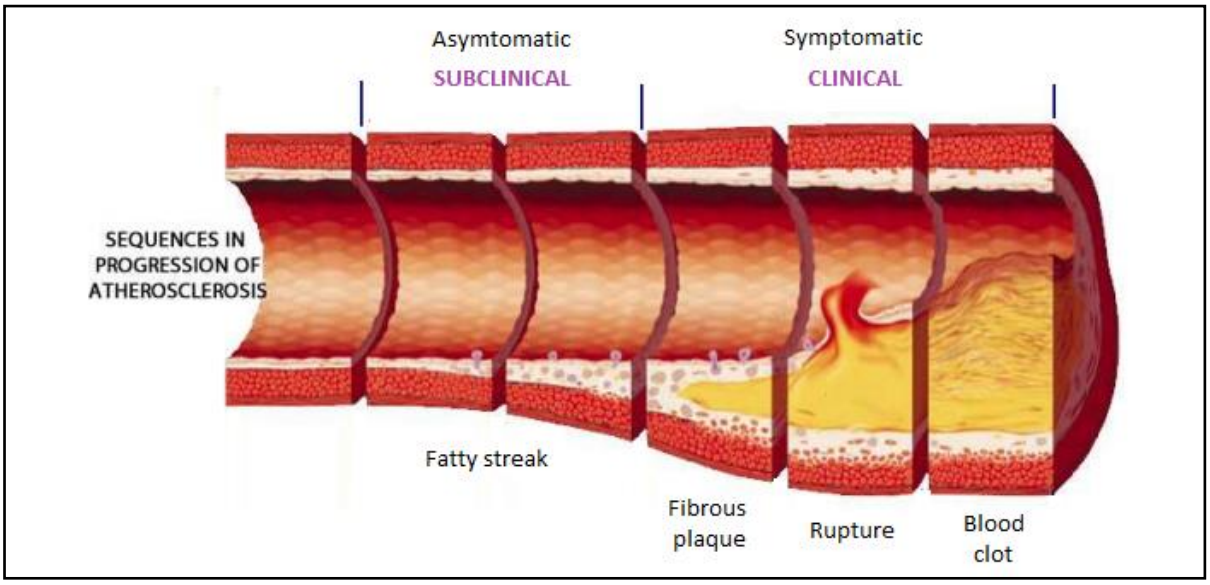

Figure 1.3. The chronological timeline of atherosclerosis. Adapted from [19].

Timeline of atherosclerosis (Figure 1.3):

Stage 1: Initiation of atherogenesis occurs as a result of endothelial lining damage in the coronary arteries. Such damage may occur due to a number of factors including shear forces, increased low density lipoprotein cholesterol (LDL-C) levels and toxins such as those present in cigarette smoke.

Stage 2: The lesion created by endothelial injury allows the influx of small molecules flowing in the blood stream. Fibrous and fatty materials such as LDL-C and smooth muscle cells infiltrate the lining and accumulate in the subendothelial space causing the formation of an initial fatty streak.

Stage 3: Once inside the lining, the LDL's are oxidised to form oxidised-LDL's which stimulate the expression of adhesion molecules including VCAM-1, ICAM-1 and E-SEL, as well as, the secretion of various chemotactic factors. This results in the quick recruitment of monocytes into the atherosclerotic site where they differentiate into macrophages. Upon accumulation of cholesterol, the macrophages form foam cells which cause the bulking of the plaque. This is known as inflammation.

Stage 4: A cycle of lesion and inflammation is created which enables the progression of the atherosclerotic plaque. As a way of responding to the lesions, a fibrous cap is formed over the damaged area consisting of a collagen and smooth muscle matrix. This produces a hard surface over the plaque which results in the stiffening of the vessel.

Stage 5: The build up of plaque causes the narrowing of the arterial vessel which consequently reduces the volume of blood and thus oxygen to the heart and brain. This can result in pain of the

chest commonly known as angina. The continuous cycle of lesions, fatty material accumulation, inflammation and fibrous cap formation leads to the continuous growth of atherosclerotic plaque.

Stage 6: The narrowing of the lumen can be further affected by rupture of the plaque. Platelets flowing in the blood adhere to the site of rupture. If they clump together, a blood clot, also known as a thrombus may form. Not only does the clot narrow the lumen, if small parts of the clot break off, they can flow via the blood stream to smaller arteries and block them. In the most severe cases, the clot can grow so large that the whole cross section of the main arteries of the brain or heart becomes blocked, leading to heart attack or stroke.

A more detailed illustration of the stepwise process of atherosclerosis development is demonstrated in Figure 1.4 below.

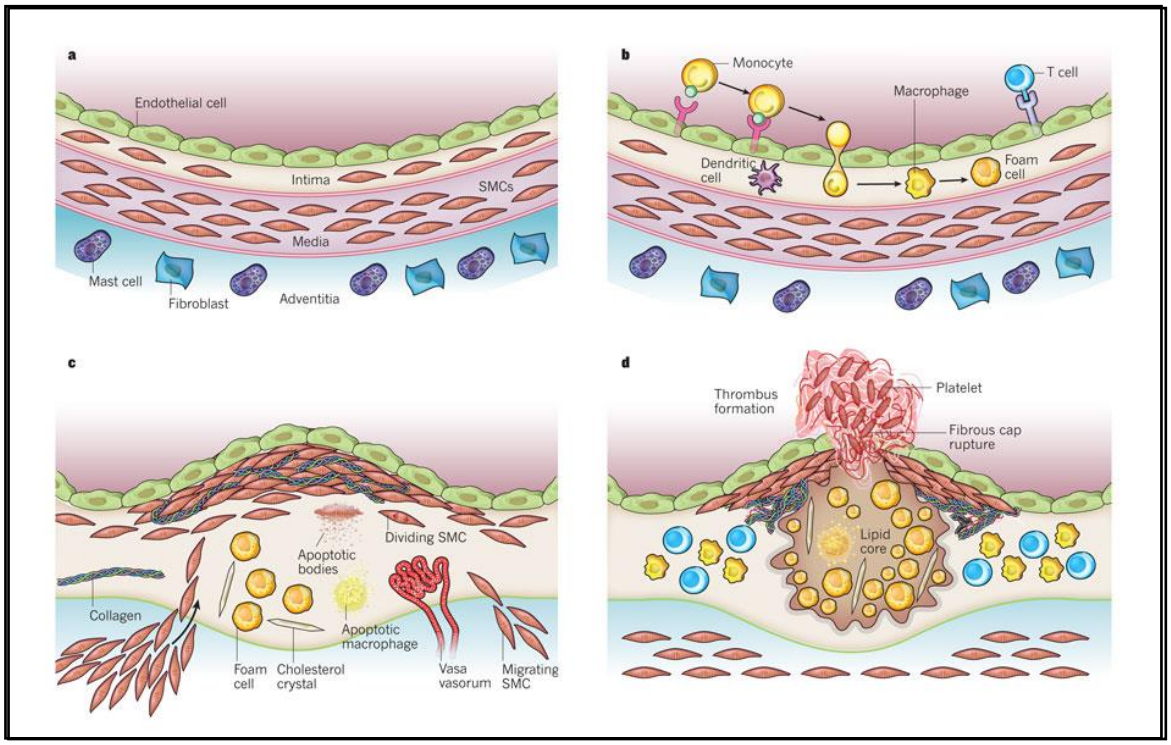

Figure 1.4. Cross sectional representation of atherosclerotic plaque progression. **a.** Normal arterial wall **b.** Endothelial damage causing the recruitment of adhesion molecules which results in the infiltration of monocytes in the subendothelial space. The monocytes are converted to macropahges which are further converted to foam cells **c.** Influx of smooth muscle cells enables the formation of a fibrous cap over the affected area **d.** Rupture of the fibrous cap allows the accumulation of platelets at site of rupture which consequently leads to formation of a thrombus. Image taken from [20].

1.2.2. Current Diagnostic Methods for Atherosclerosis

There are currently a number of methods that may be used to indicate the presence of atherosclerosis. Non-invasive methods include chest x-rays, ankle/brachial index measurements, electrocardiograms and echocardiography. Many of these imaging techniques are able to deduce a picture of the vessel lumen, however, are unable to differentiate between the plaque components. As stated by Glagov et al [21], in the early stages of atherosclerosis positive arterial remodelling occurs in order to preserve the lumen and thus visualisation of the lumen alone is not sufficient to determine whether or not atherosclerosis is present.

A leading non-invasive detection method currently being used is magnetic resonance imaging (MRI). This technique allows the visualisation of the vessel wall and unlike other lumenographic techniques is able to differentiate between plaque components [22]. Thereby, is capable of assessing plaque burden and thus indicating a state of disease. However, MRI is not without its limitations. To image an area with a cross section of several hundred microns may take as long as a few minutes. Therefore in order to cover a broad area of vessel, a substantial period of time is required. Another major limitation of the technique is that due to the presence of a magnetic field, patients with pacemakers, defibrillators or aneurysm clips are unable to enter, thus it is patient selective.

Another frequently used diagnostic method is the invasive technique of angiography, also known as cardiac catheterisation. This is where a catheter is inserted into a blood vessel usually in the groin, neck or arm through which a dye is released. An x-ray is then used to take images of the blood flow through the vessel. This technique is commonly used yet as an invasive technique, risk to the patient is increased.

Despite the abilities of the current methods for detecting atherosclerosis, there are still major limitations that must be overcome in order to detect the disease at the earliest possible stage with minimal patient distress and thus enable the best possible treatment to be provided.

1.2.3. Current Treatments for Atherosclerosis

Depending on the severity of the condition, the treatment for atherosclerosis varies. In the earlier clinical stage, medication may be sufficient to treat the underlying causes such as high cholesterol and high blood pressure. The most common drug used for decreasing cholesterol levels are statins. Their effect is to block the HMG-CoA reductase enzyme in the liver that produces cholesterol and thus reduce the overall levels in the body.

In more severe cases, surgery is often required. For example, a coronary artery bypass graft may be performed if the narrowing of the lumen is at a dangerous level. This involves the creation of a new vessel by which blood can flow to bypass the narrowed/blocked vessel. It is performed by taking grafts from the legs, arms and chest and using the tissue to make the new vessel.

It has been stated that plaque development may be halted or even regressed during the early stages of atherosclerotic development thus, as a histological stage for medical targeting, subclinical detection would give the best possible outcome of disease treatment and possible regression [23].

1.3. Nanomedicine

Nanoscale materials can be described as materials that have at least one dimension on the nanoscale; 1-100 x 10^{-9} m. The development in the production and use of nanoscale materials in medicine over the past few decades has grown at an incredible rate. Nanomaterials offer robust and sensitive platforms by which diagnostics, prognostics and therapeutics can be performed [24]. Evolution of concepts closely followed by the technology has allowed the development of highly advanced methodologies and instrumentation capable of cellular sensitive techniques. This has enabled a greater understanding of biological processes and interactions. Knowledge of such vital interactions has allowed the production of clinical methods capable of the detection of treatment of associated diseases.

Nanomedicine may be thought of as a collaboration of nanotechnology, biology, engineering, chemistry and medicine. Over the past few decades, the growth of nanomedicine has seen rapid developments in many technologies involved in disease detection, treatment and drug delivery [25]. Such advancements have dramatically changed the way in which clinical methods occur, with more robust, sensitive and specific approaches now being used.

The high sensitivity and specificity of nanotechnology when applied to medicine has been demonstrated in a multitude of studies [26-28]. Many of which utilise the functionalisation of nanomaterials with ligands which possess a high specificity for a particular target i.e. a disease biomarker. For example, an antibody which has a high affinity for a specific adhesion molecule or an oligonucleotide that will bind to a complementary nucleotide sequence. Localisation and subsequent visualisation of nanomaterials in a sample due to the presence of the target molecule has been widely used for indication of disease presence. In the case of drug delivery, the nanomaterials can localise and dispense the required drug in only the affected area, therefore reducing the effect the

drug may have on non-specific targets and surrounding bodily tissues. For example, chemotherapy is a highly effective treatment for cancer that kills cancer cells. However, it is a nonspecific technique and consequently will kill any healthy cells also in its pathway. A treatment with increased specificity, able to pinpoint the cancer cells whilst leave the healthy cells untouched would be a much more efficient treatment for cancer.

The already proven capabilities of nanomedicine, as shown by a magnitude of research studies provide scientists with great optimism of the potential future applications of nanomedicine in diagnosis and treatment of disease [29].

1.3.1. Nanoparticles

A nanoparticle can be defined as a particle with at least one dimension on the nanoscale; 1 – 100 nm. They are extremely useful as they typically show properties that are not found in bulk samples [30]. Nanoparticle samples are often referred to as nanoparticle sols or colloid. It is possible for a nanoparticle to be on the atomic scale [31].

Nanoparticle research has developed over the past few decades since their discovery in 1856 by Michael Faraday [32]. Although they were scientifically discovered in 1856, their presence within the world had been noted but had not been understood until recent decades. Nanoparticle suspensions were used subconsciously as far back as the 4^{th} Century as coatings for pots. The Lycurgus Cup is an excellent example. It was coated with a gold nanoparticle suspension to provide a glistening finish. The cup displays different colours which are dependent on the transmission of light. If light is not passed through the cup, it appears a green colour [33]. However, if light is passed through the cup, it appears red in colour.

In the last few decades, advances in nanomedicine (defined as ‘therapeutic or imaging agents which comprise a nanoparticle in order to control the biodistribution, enhance the efficacy, or otherwise reduce toxicity of a drug or biologic’) has seen the development of numerous treatments, largely based on polymeric nanoparticles. Such treatments include Adagen, Copaxone and Neulasta for severe combined immunodeficiency disease, multiple Sclerosis and neutropenia (chemotherapy induced) treatments respectively. More recent research has seen the development of micelles and protein-based nanoparticles; Estrasorb and Ontak for menopausal therapy and cutaneous T Cell lymphoma treatment respectively [34].

1.3.1.1. Surface Properties of Nanoparticles

Metal nanoparticles possess an electron cloud at their surface known as a plasmon [35]. These plasmons oscillate around the particle and upon exposure to light, speed of oscillation increases. At a specific frequency determined by the metal type and various other factors including shape, aspect ratio and surface modifications these oscillations are at their maximum, this is known as resonance. It is at this frequency that plasmon excitations occur.

When subjected to a laser at the resonance wavelength, the Raman scattering intensity is drastically increased. This effect can be further enhanced by aggregating the nanoparticles which consequently enables the coupling of surface plasmons. This in turn further increases the Raman scattering Intensity. This property can be exploited to allow the use of metal nanoparticles for detection purposes.

1.3.1.2. Nanoparticles as Probes for Detection

Previous studies have demonstrated the ability of nanoparticles to be functionalised with biomolecules such as oligonucleotides and proteins which can then be subsequently used for the purpose of detection [36,37]. Protein based nanoparticles have been utilised for the past few decades in immunocytochemistry with great success. It is in more recent year (mid 1990's) that the use of DNA conjugated nanoparticle research has soared [38]. In the case of DNA, oligonucleotides are modified with a thiol terminal group which has a high affinity for metal surfaces [39]. This results in strong chemisorption of the biomolecule onto a nanoparticle. These nanoparticle-biomolecule conjugates are known as nanoparticle probes. A variety of label/tags and analytical techniques have been used in conjunction with the nanoparticle conjugates to identify the biomarkers, including, radiolabels, fluorescent labels, surface plasmon resonance (SPR) and scanometric (chip based) methods [40]. Importantly to this project, there has been numerous studies utilising Raman reporters and SERS as the analytical technique for detection [41-43]. However, due to its low sensitivity, SERS is often not used in isolation as a sensing tool [38].

A general assay showing the function of the probes for detection is depicted in Figure 1.5. Consider a DNA sequence that codes for a specific infection. One strand is used as the target sequence whilst the complementary strand is split into two; probe 1 and probe 2. Each probe sequence is bound to two different sets of nanoparticles forming nanoparticle probes. Most commonly, synthetic oligonucleotides are modified with a thiol end group which has a high affinity for the metal surface as stated above. One set of probes is then functionalised with a Raman reporter. The reporter molecules are used in the identification process.

Once the nanoparticle probes have been formed, they are then mixed together and subjected to hybridisation with the target sequence. A non complementary sequence (also known as the nonsense sequence) is also used to act as a control. The target sequence is a single strand of oligonucleotide that is complementary to the two probe sequences and so when mixed, complementary base pairing between the sequences occurs via Watson Crick base pairing, forming a DNA duplex. This results in aggregation of the nanoparticles which allows coupling of the surface plasmons which in turn results in an increased Raman scattering intensity as demonstrated in Figure 1.5. This is referred to as 'SERS ON'. If mixed with a nonsense sequence, no hybridisation occurs, therefore no aggregation of the nanoparticles occurs thus no increase in the Raman scattering intensity is observed. This is referred to as 'SERS OFF'. Consequently there is a discriminating factor of Raman scattering intensity between SERS ON:OFF that can be exploited to determine the presence of a target sequence.

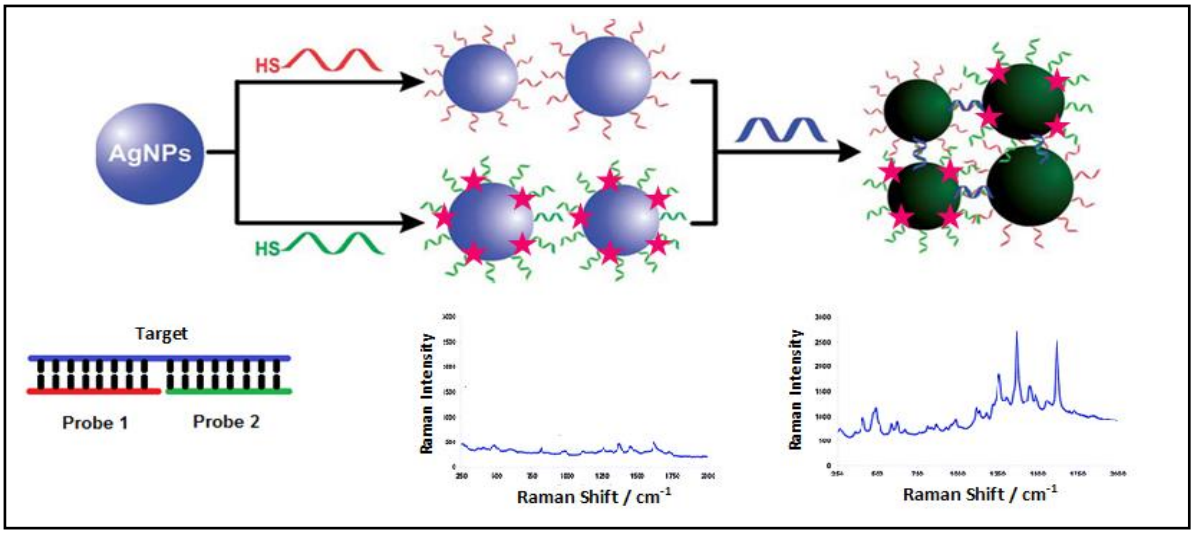

Figure 1.5. Mechanism of nanoparticle probe synthesis and hybridisation adapted from [44]. Preparation of nanoparticle probes using probe 1 (red) and probe 2 (green) with functionalisation of nanoparticle probe 2 with a Raman reporter (displayed by the pink stars). This non-aggregated form possesses a SERS OFF signal. In the presence of a target (blue) sequence, aggregation occurs turning the SERS signal ON. The ON:OFF difference can be seen by comparison of the spectra.

1.4. MicroRNAs

MicroRNA's (also known as miRNA's and miR's) are small endogenous species which play an important role in post transcriptional gene translation and expression. In 1993 during a study on the lin-4 gene in the *C. elegans* species, Victor Ambros and his fellow researchers noticed that the gene

had a repression effect on the lin-14 gene [45]. Further research and isolation of the gene enabled them to see that a protein encoding messenger RNA (mRNA) was not produced as would have been expected but instead, a short non-coding species (about 22 nucleotide bases long) was actually produced. The sequence of this oligonucleotide was found to be partially complementary to that of the lin-14 gene and thus based on the scientific observation of lin-14 repression, it was deduced that this short sequence was capable of inhibiting the transcription of the lin-14 gene. The precursor for the miRNA lin-4 sequence is shown in Figure 1.6.

Further research on *C.elegans* carried out in 2000, allowed for the discovery of another group of small non-coding RNA sequences named the let-7 family [46]. In the *C.elegans* species, a let-7 sequence was found to repress the function of the lin-41 gene. Further research into the let-7 family suggested that they were present in a variety of species including vertebrate (humans), ascidian, hemichordate, mollusc, annelid and arthropod [47]. Furthermore, they were discovered to have similar effects on control of timing and development, essentially 'housekeeping' RNA's. It was at this stage in 2001 that these species became known as microRNA's.

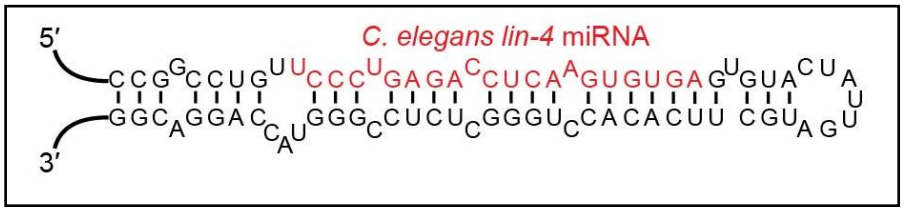

Figure 1.6. *C.elegans* lin-4 precursor sequence miRNA. Sequence in red shows the miRNA lin-4.

Over the past decade, a vast amount of research has been performed on miRNA's. Their role has been established and over 1500 sequences have been discovered in the human genome. It has been estimated via computational studies that over 60 % of total genes can be regulated by miRNA's [48]. Many of the recently discovered sequences have been critically linked to biological processes in health and disease including CVD.

1.4.1. MiRNA Synthesis

The human genome is held in the form of DNA in the nucleus of cells. The genome consists of coding and non-coding DNA. The coding DNA can be transcribed and translated to produce proteins. It is this part of the genome that is used to produce miRNA sequences via a multistage process. Firstly, a region of the DNA is transcribed to primary miRNA (pri-miRNA) via the enzyme RNA polymerase II. Pri-miRNA consists of a 5'-capped and polyadenylated tailed nucleotide sequence. The enzyme Dorsha coupled with DGCR8 then processes pri-miRNA to precursor miRNA (pre-miRNA) to form a hairpin loop structure of 70-90 nucleotide bases long. This occurs in the nucleus. The pre-miRNA is

then transported to the cytoplasm by Exportin-5. In the cytoplasm it is further processed by RNA polymerase III enzyme Dicer to form a mature-miRNA duplex. The duplex of approximately 22 bases consists of two complementary single strands; miRNA and miRNA*. The single stranded mature-miRNA (miRNA) is incorporated into an RNA sequencing inducing complex (RSIC) whilst the complementary strand (miRNA*) is degraded. Once incorporated into the RSIC, the act of gene translation repression or blockage can be performed. An illustration of this synthesis is displayed in Figure 1.7.

It is thought that translational repression occurs since the miRNA possesses a partially complementary base sequence to a region of the targeting gene. Via Watson-Crick complementary base pairing the miRNA binds to the 3'-UTR region of the protein encoding mRNA transcript and as the ribosome moves down the RNA sequence during the process of translation, it is halted by the presence of the miRNA and thus no further translation can occur.

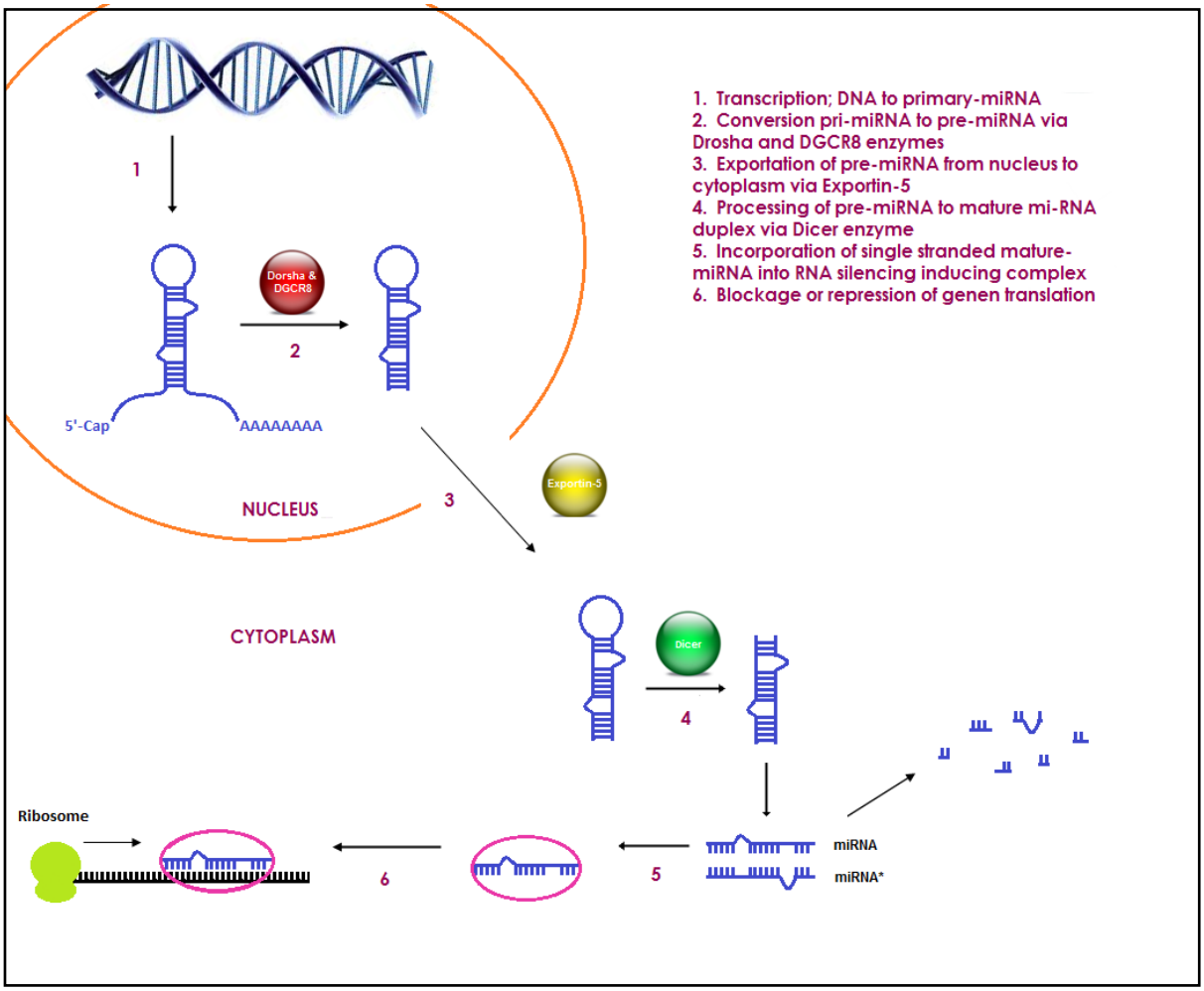

Figure 1.7. Schematic showing the step by step process of miRNA synthesis

1.4.2. Circulating MiRNAs

One of the main reasons miRNA's have become a pivotal area of research is their presence in the circulatory system. Although present at an intracellular level as with DNA and other RNA's, miRNA's have been found to circulate in the blood. This is unusual as also present in the circulatory system are large amounts of enzymes capable of nucleotide destruction. Studies have shown that under harsh conditions of boiling, extreme pH and multiple freeze-thaw cycles plasma miRNA's were found to remain stable [49]. Yet, when synthetic miRNA sequences were added exogenously, they were instantly degraded. This therefore suggests that the endogenous miRNA's are somehow protected from the RNase enzymes present in the sample. Recent studies have suggested two main mechanisms by which this stability may arise. The first being encapsulation within microparticles such as exosomes, vesicles and apoptotic bodies to produce a protective layer around the miRNA's and the second explanation being conjugation to proteins such as Ago2 or high density lipoproteins [50-52]. This extreme stability of miRNA's in blood plasma has rendered them as perfect targets for diagnostics and prognostics of disease.

The knowledge of their ability to finely regulate gene expression has enabled the exploration of the idea of exploitation of such sequences in order to manipulate the regulation of genes which are involved in the pathogenesis of disease, thereby control the state of disease.

1.4.3. MiRNA's in CVD

Since the discovery of miRNA's, research into their role in biological processes of a range of diseases has been undertaken. Significantly to this project, a keen focus area has been on their involvement in the pathogenesis of CVD.

The role of miRNAs on post transcriptional regulation has shown to be essential for the maintenance of cardiac homeostasis [53]. Both in vivo and in vitro models have enabled the discovery of the role of a number of different miRNA sequences within the cardiovascular system.

Studies on mice models have displayed the role of miRNA's during heart development. MiRNA-1 and miRNA-133 have been shown to play a vital role in cardiac development by controlling the balance between differentiation and proliferation of cardiac cells [54]. Therefore unsurprisingly, further studies have shown that under cardiac stress or damage, this gene programme is reactivated and subsequently reactivation of corresponding miRNA's occurs in order to regenerate the heart [53].

Further studies have enabled the discovery of a number of miRNA's to work in a similar manner. Many were found to be related to a range of diseases such as the let-7 family were found to be

regulated in cancers and CVD's. A number of sequences were found to have high specificity for the different types of CVD's as highlighted in Table 1.1. There are two possible correlations between miRNA's and disease progression; an increase in number or a decrease in number; upregulation and downregulation respectively. When there is no correlation between the two, it is classed as no effect. This response of the production or degradation of miRNA sequences has demonstrated the fine control the short oligonucleotide sequences have on the regulation of biological functions in response to disruption or abnormalities.

MiRNA's have been shown to exert great control over the functions of endothelial, smooth muscle and macrophage cells. Such functions are involved in the multiple stages of plaque development and thereby, miRNA's have some implication in the pathogenesis of atherosclerosis. From the initial stage of endothelial lining damage, endothelial rich miRNA's including miR-126, miR-31 and miR-17 are present to regulate the inflammation process. They do so by controlling the expression of adhesion molecules VCAM-1, ICAM-1 and E-SEL which are produced in response to the presence of LDL's in the arterial wall.

Condition	**MiRNA**	**Upregulation/Downregulation**
Acute Myocardial Infarction	1, 133, 208a	Upregulated
Heart Failure	126 7-family 499	Up&Down regulated recorded Upregulated Upregulated
Cardiac Hypertrophy	21, 23a, 125, 129 1, 29, 133	Upregulated Downregulated
Vascular Diseases	126	Downregulated
Cardiac Fibrosis	21 29	Upregulated Downregulated

Table 1.1. Table of CVD specific miRNA's.

Plaque development occurs via the uptake of lipids from circulation, the levels of which are controlled by the expression of SREBP2/1a gene. It was recently found that miR-33a/b regulate the metabolism of cholesterol and other fatty acids, thus the levels of such fats in circulation [55,56]. Once inside the intima, the lipids are oxidised and loaded into monocytes/ macrophages producing foam cells. This is the inflammatory response, creating the bulk of the plaque. This response is governed by miR-155 and miR-125a-5p [57]. The formation of the fibrous cap involves the migration

and differentiation of smooth muscle cells thus is controlled by miRNA's which control the function of SMC's such as miR-26a, miR-221 and miR-222 [48].

As shown by the research presented above, a vast number of miRNA's relating to the regulation of cardiac homeostasis have been discovered and no doubt more will be discovered in the near future. Their intimate ability to fine tune the expression of genes relating the progression of atherosclerosis expose them as extremely promising targets for therapeutic diagnosis and treatment of CVD.

1.4.4. MiRNAs as therapeutic targets

MiRNA's have exposed themselves as potentially powerful diagnostic biomarkers. Correlations between levels of miRNA's in both tissue and blood samples has been demonstrated to be linked with the presence and in some instances, stage of a disease.

The ability to detect and quantify the presence of pathogenetic miRNA's may allow the possible detection of diseases. This would involve the extraction of miRNA from a sample, identification of sequences and further quantification to indicate the levels present and thus infer the presence, absence or state of disease.

2. Objectives

The main aims of this project can be split into two parts;

The first aim is to create an assay capable of the detection, identification and quantification of CVD specific circulating miRNA. This will be expanded into a multiplexed detection system, whereby a number of different CVD linked miRNA sequences can be simultaneously identified.

The second aim is to prepare functionalised nanoparticles capable of cell layer penetration. The overall aim for this is to use hollow gold nanoparticles as a transport medium for drug delivery or biological component identification/location in atherosclerotic plaques. For the purpose of this study, solid gold nanoparticles will be used.

3. Experimental

3.1. Nanoparticle Synthesis and Characterisation

3.1.1. Materials

Silver nitrate, sodium tetrachloroaurate, hydroxylamine hydrochloride, sodium hydroxide, sodium citrate. All chemicals purchased from Sigma Aldrich.

3.1.2. Nanoparticle Synthesis

For this research, both solid silver and solid gold nanoparticles were used. Silver nanoparticles were initially used due to their easy preparation, high stability and higher SERS efficiency, thus allowing a greater SERS signals to be obtained [58]. This allowed the concept of this research to be investigated more easily; ON:OFF SERS signals to be more recognisable. However, silver nanoparticles have shown to have toxic effects when inside the human body [59]. Therefore, once the technique was established, gold nanoparticles were substituted in place of the silver nanoparticles. Gold nanoparticles have proven to have good cellular uptake and lower toxicity and thus for biological compatibility reasons, gold nanoparticles were used for the remainder of this research [60].

Silver; The synthesis method used followed the hydroxylamine hydrochloride reduction of silver nitrate as outlined by Leopold and Lendl in 2002 [61].

A 270 mL hydroxylamine hydrochloride/sodium hydroxide (1.67×10^{-3} M and 3.33×10^{-3} M respectively) solution was prepared in a glass vessel. This was done by adding 270 mL of deionised water to the vessel. 0.0313 g of hydroxylamine hydrochloride and 0.0360 g of sodium hydroxide were weighed out in Eppindorfs. Each solid reagent was then dissolved in approximately 1 mL of water taken from the vessel and the dissolved solution was then added back to the vessel. A further 1 mL of the vessel solution was used to wash the Eppindorfs and the washings were added back into the solution. This ensured all of the solid reagents weighed out were transferred to the solution and thus the concentration was as accurate as possible.

A 30 mL silver nitrate solution at 10^{-2} M was prepared by adding 0.0507 g of silver nitrate to 30 mL of deionised water. This solution was then added quickly in 1 mL aliquots to the above solution whilst being moderately stirred using a magnetic stirrer bar. Once all the silver nitrate solution had been added the solution was left to stir for a further 15 minutes.

Gold; The synthesis method used was based on the Turvekich method for the synthesis of gold nanoparticles by the citrate reduction of gold chloroaurate solution [62]. A 1 L three necked round bottom flask and glass rod stirrer were soaked in aqua regia (concentrated nitric acid : concentrated hydrochloric acid 1 : 3 v/v) for 24 hours prior to nanoparticle synthesis.

500 mL milli-Q water was added to the flask along with 50 mg sodium tetracholoaurate. The solution was heated until boiling. With vigorous stirring, 0.075g sodium citrate in 7.5 mL water was added. The solution was boiled for a further 15 minutes with foil covering the neck openings to maintain the volume. After 15 minutes, the heat was turned off and the solution was allowed to cool, maintaining constant stirring.

3.1.3. Nanoparticle Characterisation

3.1.3.1. DLS Analysis

Synthesised nanoparticles were sized using the Malvern Zetasizer Nano ZS90. The instrument was calibrated upon start-up using a 40 nm latex standard. Once the calibration was complete 1 mL of nanoparticle sample was analysed in a plastic cuvette. The data gained from the nanosizer was then used to select the appropriate molar extinction coefficient value from the literature, which is used in the UV-Vis analysis to calculate concentration as described below [63,64].

3.1.3.2. Extinction Spectroscopy

Extinction spectroscopy was performed in order to calculate the concentration of the nanoparticle sample from the λ_{max} of the sols. All analyses were performed using a Cary 300 Bio or Perkin Elmer UV-Visible spectrophotometer with a wavelength range of 200 – 800 nm, a collection time of 0.1 s, a scan rate of 600 nmmin^{-1} and a 1 nm resolution. These settings were used for all extinction spectra obtained during this research.

The general procedure used to perform this analysis was as follows. Initially a background was ran using 400 µL of sample suspension liquid. The sample was then ran at an appropriate dilution to ensure a λmax value of less than 1.

The absorbance and wavelength values at the λ_{max} point of the extinction spectrum were noted and used to calculate the concentration of the sample, using the molar extinction coefficient value determined from the nanosizer data. Values of $2.87\ x\ 10^{10}\ \mathrm{mol}^{-1}\mathrm{dm}^{3}\mathrm{cm}^{-1}$

(based on the closest comparable size of 40 nm particles) and 7.941 x 10^8 (based on the closest comparable spherical size of 19 nm gold particles) for silver and gold particles respectively [63].

Also, the full width half maximum (FWHM) was determined by taking the difference in wavelength values of the two values of the peak line that lie at half the peak height value. This was performed to identify the polydispersity of the sample.

3.2. MiRNA Detection

3.2.1. Matertials

DNA and RNA sequences were purchased from IDT and atdBio. LNA sequences were purchased from Exiqon. Synthetic serum was purchased from CST Technologies.

3.2.2. Solution MiRNA detection

Solution based miRNA detection was based on a two stage process; conjugate (nanoparticle-probe) synthesis followed by hybridisation and SERS analysis.

3.2.2.1. Conjugate Synthesis

Below outlines the general protocol for synthesising nanoparticle-probe conjugates. Adaptations based on this method were performed.

1 mL of nanoparticle sol was mixed with 1 mL of water in two separate vials labelled 'Probe 1' and 'Probe 2' (P1 and P2). X µL of oligonucleotide (probe) 1 is added to the vial labelled P1 and X µL of oligonucleotide (probe) 2 is added to the vial labelled P2. (5000 oligonucleotides per nanoparticle were used throughout this project). The vials were then shook for 10 mins. 80 µL of 250 mM sodium citrate buffer pH 3 solution was added to each vial and shaking continued for at least half an hour. Each vial was then split into two Eppendorfs and spun using a centrifuge at 5000 rpm for 20 mins. The supernatant was discarded taking care not to disturb the pellet which was then resuspended in 1 mL of water. Since there were two Eppendorfs per probe, one pellet was initially resuspended in the 1 mL of water and the contents transferred to the second Eppendorf and the second pellet resuspended in the same 1 mL. An extinction spectrum of P2 was collected to determine the nanoparticle-probe concentration, which was then used to calculate the volume of dye required. The volume of dye required, was calculated using the Beer-Lambert equation, the concentration of dye and the number of dye molecules per nanoparticle required. (The number of dye molecules per nanoparticle varied depending on the dye used). Once calculated, X µL of dye was added to the P2 sample and shook for 15 minutes. Both P1 and P2 Eppendorfs were then spun at 5000 rpm for 20

mins. Again the supernatant was discarded and the pellet resuspended in 1 mL of 0.1 M phosphate buffer saline (PBS). Extinction spectra were collected, this time on both P1 and P2 and the data used to calculate the volume of each oligonucleotide-nanoparticle conjugate required to prepare a 10 pM solution of conjugate in 150 µL which is then used in the SERS analysis.

(Note the volumes of oligonucleotide and dye required were calculated based on the extinction spectra using the Beer-Lambert law).

3.2.2.2. Hybridisation Procedure

Once the conjugates were synthesised, they were then subjected to hybridisation by mixing with a target sequence. Controls were performed by mixing with a nonsense sequence or no sequence where no hybridisation should occur.

The hybridisation conditions utilised for solution phase hybridisation were as follows; 10 pM of nanoparticle-P1, 10 pM of nanoparticle-P2, 10 nM of Target/Nonsense (or equivalent volume of control) and the remaining volume to make 150 µL of 0.3 M PBS (0.3 M NaCl 10 mM phosphate buffer). The appropriate volumes required to make these final concentrations was calculated based on the NP-probe conjugate concentration determined via extinction spectroscopy.

For example; 7.35 µL NP-P1 + 6.25 µL NP-P2 + 6 µL target/nonsense + 130.40 µL 0.3M PBS. Makes a total volume of 150 µL.

8 x 150 µL mini vials were used to prepare the hybridisation samples as above in the order of; NP-P1, NP-P2, PBS and finally the target/nonsense sequence. A cap strip was used to secure the vials and they were briefly vortexed then left to hybridise for at least 30 minutes. Note that a nonsense sequence was not always used and instead 6 µL 0.3 M PBS was used to keep volumes and thus concentrations consistent. Prior to SERS analysis the samples were briefly spun in a mini centrifuge to draw the entire sample to the bottom of the Eppendorf and was then transferred to a well plate for SERS analysis.

Initially, hybridisation with model DNA-DNA duplexes was performed (which have previously been shown to work) in order to ensure the hybridisation mechanism was effective. Once proven to work, a variety of nucleotide duplexes were exploited to investigate the ability to detect miRNA sequences.

3.2.2.3. SERS Analysis

The contents of the mini vials were dispensed into a 96 well plate for analysis on the Renishaw Plate Reader instrument. All spectra were collected using a 532 nm laser with a Raman shift range of 250 – 3000 cm^{-1} at 0.50 cm^{-1} intervals with an exposure time of 1s. The instrument was calibrated using an

internal silica standard. The laser was focused using 150 µL of ethanol to optimise the distance between the objective and the sample by attaining the highest signal intensity for the 2729 cm^{-1} peak.

3.2.3. Hybridisation Experiments

A series of hybridisation experiments were performed, each working off the previous experiment. (Note that duplex notation follows probe-target structure e.g. DNA-DNA refers to DNA probes with DNA target).

Experiment 1. Model DNA-DNA. This was performed as previous work has shown successful hybridisation of these sequences with a significant resulting ON:OFF SERS signal difference observed. Thereby, achievement of this signal would show the hybridisation method to be effective and thus allow subsequent experimentation using the same method.

Experiment 2. Model DNA-RNA. Once the DNA target had been proven to be effective, an RNA target of the same sequence was used.

Experiment 3. DNA-miRNA-146a. Once the model sequences were proven to hybridise efficiently and provide a significant ON:OFF difference in the SERS spectra, movement was made to look at miRNA as a target. A sequence taken from the literature shown to be linked to CVD was initially used as a miRNA target; miRNA-146a Homo Sapien (miR-146 HS).

Experiment 4. LNA-miRNA-214. The next step was to create a hybrid with higher hybridisation efficiency. For this, the use of LNA (locked nucleic acid) was employed. LNA modified probes were custom synthesised with every fourth base modified with an LNA base. A different miRNA sequence, also shown in the literature to be linked to CVD was used as the target; miRNA-214.

Sequence	P1	P2	Target
Model	TCTCAACTCGTA	CGCATTCAGGAT	TACGAGTTGAGAATCCTGAATGCG DNA
			UACGAGUUGAGAAUCCUGAAUGCG RNA
miRNA-146a HS	THIOhexyl//3xHEG/TTCAGTTCTCA	THIOhexyl//3xHEG/AACCCATGGAA	UGAGAACUGAAUUCCAUGGGUU miRNA
miRNA-214	ThioMC6-D//iSp18/**A**CTG**C**CTG**T**CT LNA	ThioMC6-D//iSp18/G**T**GCC**T**GCT**G**T LNA	ACAGCAGGCACAGACAGGCAGT DNA ACAGCAGGCACAGACAGGCAGU miRNA

Table 3.1. Base sequences for the probes and corresponding target sequences. For miRNA-214, the LNA bases present in the probes sequences are represented in bold.

3.2.4. Kinetics

Kinetic experiments were performed in order to determine the rate of hybridisation for a number of duplexes. All experiments were performed on the Cary 300 Bio UV-visible spectrophotometer with a wavelength range 200 – 800 cm^{-1} with 10 cycles for 60 seconds and a collection time of 1 second.

3.2.5. Hybridisation Vs Time Study

A series of experiments were conducted to observe how the rate of hybridisation alters with time. All experiments were performed on the Renishaw Plate Reader with a 532 nm laser. Spectra were collected every 10 minutes after an initial 30 minutes hybridisation period with a Raman shift range of 250 – 3000 cm^{-1} at 0.50 cm^{-1} intervals and an exposure time of 1s.

Duplexes for which hybridisation Vs time studies were performed; Model DNA – DNA, Model DNA – RNA and DNA – miRNA.

3.2.6. Serum Doping

The next stage was to perform the hybridisations in a matrix closer to that of biological fluid. This was performed by doping synthetic serum into the hybridisation samples. Synthetic serum was purchased from CST Technologies.

Repeat experiments were performed using the following doping compositions;

Hybridisation Matrix Composition Volumes (%)	
0.3 M PBS	**Synthetic Serum**
100	0
80	20
60	40
40	60
20	80
0	100

Table 3.2. PBS:Synthetic serum hybridisation compositions

3.3. Cholesterol Covered Nanoparticles

3.3.1. Materials

Custom designed 5’ thiol, 3’ cholesteryl TEG modified 12xT oligonucleotide purified via PAGE purchased from atdBIO. Model probe 2 oligonucleotide purchased as above.

3.3.2. Synthesis

Two methods were utilised for the synthesis of cholesterol covered nanoparticles. Both followed a similar method to the fast conjugate synthesis as described in '3.2.2.1 Conjugate Synthesis'. The oligonucleotide- cholesterol TEG moieties used were 12xT-Cholesterol-TEG with a C6-thiol modified 5' end. (oligo-cholesterol coverage was performed at a calculated total of 5000 oligo's per nanoparticle).

Method 1

Step 1: Functionalise nanoparticle with oligo-cholesterol

↓

Step 2: Add dye

Method 2

Step 1: Functionalise nanoparticle with dye

↓

Step 2: Add oligo-cholesterol

In both methods, the addition of cholesterol was closely followed by the addition of sodium citrate buffer pH 3. After each addition, the sample was spun at 5000 rpm for 20 minutes to remove any excess dye/oligo-cholesterol.

Initially, 100 % cholesterol covered nanoparticles were synthesised.

Then a series of mixed monolayer's consisting of a model probe and cholesterol sequences were prepared according to the compositions in Table 3.2.

Percentage Coverage (%)	
Model Probe	**Oligo-cholesterol**
100	0
50	50
0	100

Table 3.3 Surface coverage compositions of cholesterol covered nanoparticles.

3.3.3. Characterisation

3.3.3.1. Extinction Spectroscopy

Extinction spectra were obtained on a Perkin Elmer or a Cary 300 Bio UV-Visible spectrometer. All spectra were taken with a wavelength range of 800 – 200 cm^{-1} and a collection time of 0.1 s with a scan rate of 600 $nmmin^{-1}$ at 1 nm resolution.

3.3.3.2. Size Measurements

DLS measurements were performed on the Malvern Zetasizer Nano ZS90. For size measurements, the instrument was calibrated with a 40/20 nm polystyrene latex standard. Sample measurements were performed with 120 seconds equilibration time, 3 average values derived from a mean of 14 separate measurements.

For zeta measurements, the instrument was calibrated using a zeta potential transfer standard (-42 mV ±4.2 mV).

3.3.3.3. Gel Electrophoresis

Gel electrophoresis was carried out on a 1 % agarose gel. The gel was prepared by adding 1 g of agarose powder to a 10x Tris/Borate/EDTA (TBE) buffer solution (10 mL 100x TBE solution to 90 mL water). The solution was heated in a microwave for 3 minutes to dissolve the agarose and the hot solution was then poured into the prepared gel chamber. A comb was placed in the top end of the chamber and the gel was left to set.

The electrolyte used was 10x TBE. A gel was run at around 165 volts for about 90 minutes.

3.3.4. Biological Activity of Cholesterol Covered Nanoparticles

Firstly the particles were tested for their stability in cell media. This was performed by spinning the particles down and resuspending the pellet in media.

The particles were then incubated in macrophages. The cell line used for this experimentation was RAW 264.7 murine macrophages. The cell medium used was DMEM with 10 % FBS. The cells were subcultured in T-175 flask, then reseeded in a 30 mm petri dish with cover slide for nanoparticle treatment. 400 µL of NP sample was applied to each dish. The slides were washed three times with PBS and then left to air dry.

2-dimensional Raman images were achieved using a WITec alpha 300R confocal Raman microscope with a helium-neon 633 nm laser and lens-based spectrometer with CCD detector cooled to -60 °C. Various image sizes were taken, each with a spectral matrix of 1 micron steps, integration time of 1 second and variable laser powers were used. The instrument was calibrated using a silica standard and the mapping axes calibrated using the automated rotation correction feature in the WITec software. Samples were focused using the field stop to optimise the distance between the sample and the laser.

Four samples were prepared and analysed according to the method above; 1.Bare nanoparticle, 2.Nanoparticle + Cholesterol mix and 3 Nanoparticle + Malachite Green + Cholesterol mix. A control of bare cells was also prepared.

4. Results and Discussion

4.1. Nanoparticle Synthesis and Characterisation

4.1.1. Synthesis

Silver synthesis: The Leopold and Lendl method of hydroxylamine reduction was chosen due to its quick and easy synthesis procedure. From start to finish, the total synthesis can be performed within an hour. This method was also chosen was due to its reported ability to synthesise reproducible monodisperse nanoparticle samples [61]. This is important as multiple batches of colloid was required for this work and for the purposes of any future work, to ensure consistency and reproducibility of results, the nanoparticles used must be of similar properties.

Gold synthesis: The Turkevich method of citrate reduction for the synthesis of gold nanoparticles was chosen also due to the ease of synthesis and the consistency of the method to prepare reproducible particle samples. The precise control the amount of citrate added has on the size of the resulting particles, also allowed for the manipulation of specific particle sizes to be synthesised.

For the miRNA studies, silver nanoparticles were used due to their increased plasmon excitation efficiency which renders an increased SERS sensitivity when compared with gold [65]. The greater sensitivity should allow for a greater difference in the ON:OFF SERS signal to be achieved which is subsequently used to detect the presence of a target sequence. Also, an increased sensitivity means that silver has a greater potential to detect trace quantities which consequently allows smaller sample sizes to be analysed. This would be advantageous when dealing with biological samples such as the application of this project.

For the cholesterol covered nanoparticles, gold particles were used. This was due to their compatibility with biological samples [66]. Gold nanoparticles have shown to be relatively inert to cells whilst silver has shown to be toxic to cells [67].

4.1.2. DLS Analysis

A number of batches of silver nanoparticles were synthesised and used throughout this project. The nanosizer determined the average diameters of the particles to be within the range of 32.38 – 45.86 nm. From these values the molar extinction coefficient value for all batches was estimated to be $2.87\ x\ 10^{10}\ \mathrm{mol^{-1}dm^{3}cm^{-1}}$ (taken from the literature for closest comparable size of 40 nm particles) [63].

One batch of gold nanoparticles was synthesised and used during this work. The average particle size was 18.58 nm. From this, the molar extinction coefficient was estimated to be 7.941 x 10^8 (value for closest value of spherical 19 nm gold particles).

4.1.3. Extinction Spectroscopy

Extinction spectroscopy was used to calculate the concentration of nanoparticles in solution. This was calculated using the λ_{max} absorbance value and the molar extinction coefficient determined from the nanosizer data with the Beer-Lambert law (equation 3). Example extinction spectra of silver and gold nanoparticles are shown in Figure 4.1.

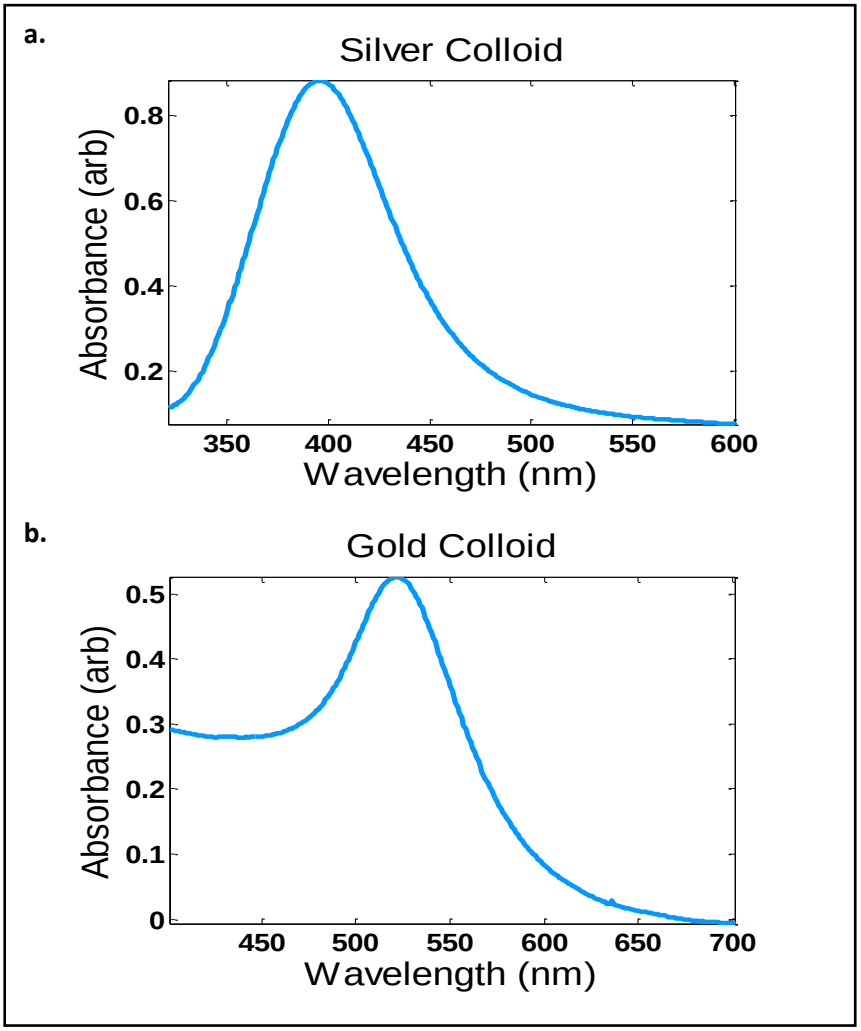

Figure 4.1. Extinction spectra for **a.** silver nanoparticles (hydroxylamine reduced); λ_{max} value of 396 nm **b.** gold nanoparticles (citrate reduced); λ_{max} value of 521 nm.

$$A = \varepsilon c l \tag{3}$$

Equation 1. Beer-Lambert law where A = absorbance, ε = molar extinction coefficient (mol^{-1} dm^3 cm^{-1}) c = concentration ($moldm^{-3}$) and l = pathlength (cm).

4.2. Solution Phase miRNA Detection

4.2.1. Conjugate Synthesis

The method used for conjugate synthesis in this project differs to reported methods due to its highly efficient and time saving ability to synthesise stable oligonucleotide–nanoparticle conjugates with high reproducibility. In total, the synthesis takes around 4 hours to complete, comparatively far quicker than traditional salt aging methods. Therefore less cost, time and labour is required.

Citrate buffer (pH 3) was added to the nanoparticle and oligonucleotide solution to lower the pH of the solution to around pH 4.5. This was necessary in order to remove the stabilising agent off the surface of the nanoparticle and allow the subsequent binding of the oligonucleotides onto the now free surface. Upon centrifugation and resuspension in water a neutral pH was restored.

The final pellet was resuspended in 0.1 M PBS. This was performed to place the conjugates in physiological conditions and better mimic real life samples.

4.2.2. Hybridisation and SERS

The next stage of the assay was to use the newly synthesised conjugates to identify the presence of a target sequence. This was performed via a hybridisation process involving two nanoparticle-probe conjugates and a complementary (target) sequence. Separate samples with a non-complementary (nonsense) sequence were used to act as a control for samples where no hybridisation should occur. The mechanism by which hybridisation occurred followed a head to tail structure. A schematic demonstrating this mechanism is displayed in Figure 4.2.

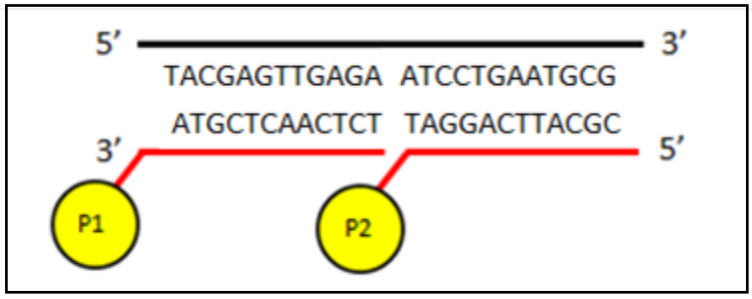

Figure 4.2. Schematic showing head to tail hybridisation mechanism of nanoparticle-probe conjugates.

In the presence of a complementary target sequence, hybridisation should occur between the complementary base pairs via Watson-Crick base pairing. This causes the probe associated nanoparticles to come within close proximity of each other which subsequently allows coupling of the nanoparticle surface plasmons via delocalisation of the surface electrons. This in turn increases

the Raman scattering intensity. This is known as 'SERS signal ON'. In the presence of a nonsense sequence, no hybridisation should occur, thus no aggregation of nanoparticles and consequently no increase in Raman scattering intensity should be observed. This is known as 'SERS signal OFF'. In order for a positive identification of a target sequence to be declared, an ON:OFF Raman signal must be observed with sufficient difference in intensity. It is this difference in intensity that provides the characteristic by which the identification of a target sequence is determined. An example spectrum showing an ON:OFF signal difference is displayed in Figure 4.3.

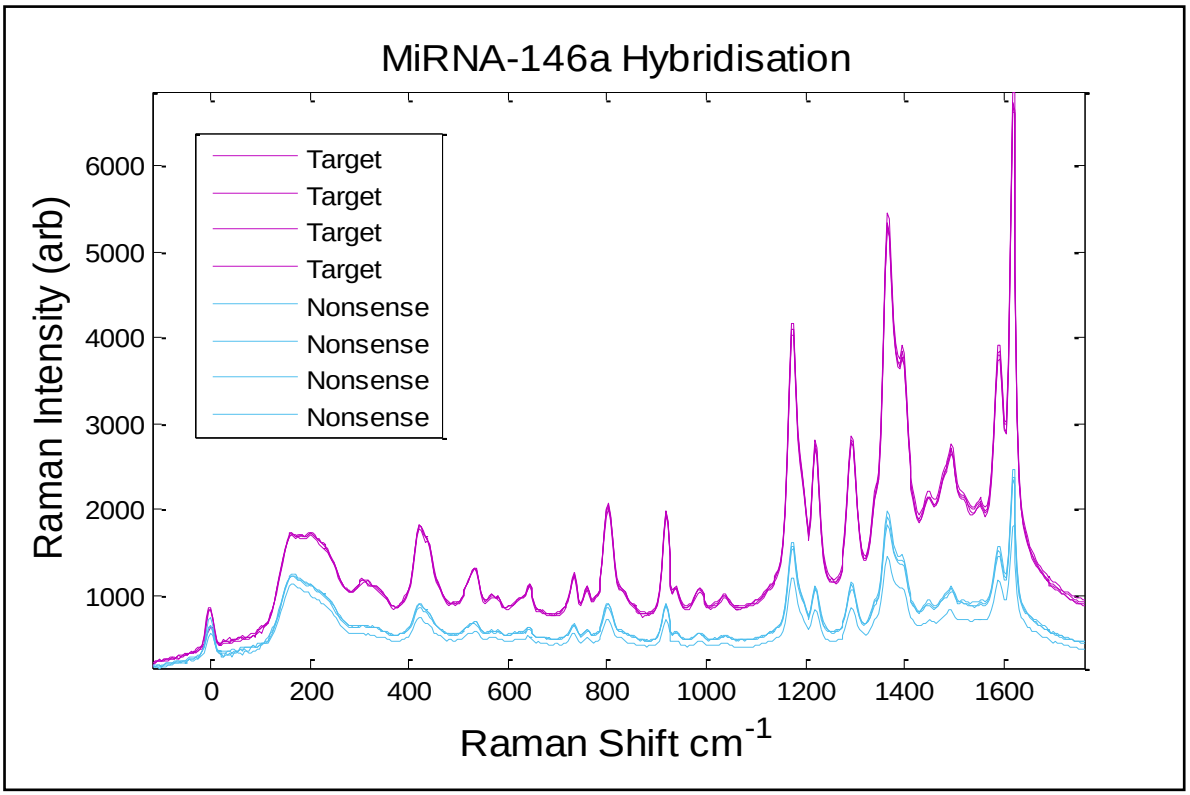

Figure 4.3. Example spectra displaying ON:OFF signal intensity difference. miRNA-146a duplex (DNA probes with miRNA target).

Despite hybridisation not occurring in the presence of a nonsense sequence, a signal was still observed. The exact reason for this is unclear, yet there are a number of possible explanations. Firstly, functionalisation of a nanoparticle with a Raman reporter alone has a SERS effect and so when excited with a Raman laser, the roughened metal surface will allow a signal of the reporter molecule to be obtained. Another reason may be that random base pairing between probes may occur causing slight aggregation of the nanoparticles and consequently increase the SERS effect. Finally, if not completely stable, the nanoparticles may slightly aggregate and thus slightly enhance the SERS effect.

In order to achieve the optimum ON:OFF signal, the ON signal must be maximised whilst the OFF signal must be minimised.

4.2.3. Hybridisation Experiments

Experiment 1. Model DNA-DNA- Initial hybridisation experiments were performed using a model DNA duplex which has been previously shown to work effectively and provide a sufficient ON:OFF SERS signal [68]. This allowed the hybridisation method to be tested for effectiveness. A large number of repeats were performed involving the model DNA-DNA duplex, each time a successful ON:OFF signal was observed with a reliable intensity difference.

Experiment 2. Model DNA-RNA- The next stage was to use the same model system with DNA probe sequences as in experiment 1, but this time use an RNA target sequence. This better mimicked miRNA which is the ultimate target of detection for this project. The exact same conditions were employed and again a large number of repeats were performed, each time yielding spectra with reliable ON:OFF signals.

Experiment 3. DNA-miRNA-146a (Homo Sapien; HS) - Once the model systems had been proven to be effective, a miRNA sequence taken from the literature shown to be linked to CVD was then utilised as a target sequence [48, 69, 70]. MiRNA-146a has been shown to be upregulated during the progression of atherosclerosis [69]. Studies show that the miRNA-146a sequence plays a role in the aging of endothelial cells [71] but more importantly to this project, the sequence has been shown to have an important role in the pro-inflammatory response. This is as a result of the nuclear factor kappa B which is heavily involved in the intracellular signalling response to inflammation [72]. Scientists have exploited this knowledge and produced a treatment for patients with coronary artery disease of statins (atorvastatin) and angiotensin II receptor blockers which decrease the circulating levels of miRNA-146a and consequently exert the anti-inflammatory response required [69].

All spectra obtained from hybridisation experiments involving the miRNA-146a target displayed distinctive ON:OFF signals. When compared to the model DNA-DNA spectra, the overall Raman intensity was substantially lower with a general intensity about half that of the model spectra. However, despite this, the relative intensities still produced a sufficient ON:OFF signal ratio and consequently the ability to state the presence of a target sequence could still be performed.

Experiment 4. LNA-miRNA-214 – The next stage was to attempt to improve the ON:OFF signal ratio by improving the hybridisation efficiency. Literature has reported the use of locked nucleic acids (LNA's) as a form of DNA probe that has a greater hybridisation efficiency to a target sequence than a standard DNA probe [73-75]. Initial experiments were carried out using the same conditions as for all previous hybridisation experiments. When this was performed, no ON:OFF signal was observed.

In response to this, the buffer utilised was altered. 1 M NaCl 20 mM phosphate solution was prepared and used in the hybridisation procedure. The purpose of a high salt hybridisation buffer is to allow for increased base pair formation. A high salt, low temperature hybridisation buffer has a low stringency effect whereby sequences with slight mismatch may still hybridise. Whereas, a low salt, high temperature hybridisation buffer has a high stringency effect and allows only for exact sequences to hybridise.

When a high hybridisation buffer was used, an ON:OFF signal was observed with the complementary signal at a higher average intensity than when no target was present. However, the difference between the signals was minimal and so the presence of a target sequence could not be stated with confidence.

The results obtained from the LNA experiments did not reflect the higher hybridisation efficiencies stated in the literature. Since the LNA probes did not provide the efficiency required and were considerably more expensive than the DNA probes, the LNA probes were no longer used for any further experimentation.

4.2.4. Kinetics

Kinetic experiments were performed to show the rate at which aggregation occurs during the hybridisation process. As hybridisation occurs, the nanoparticles aggregate which results in an increase in particle size which in turn alters the optical properties of the particles. This may be observed as a decrease in absorbance intensity and a shift in wavelength. The results from a single kinetics study are shown in Figure 4.4.

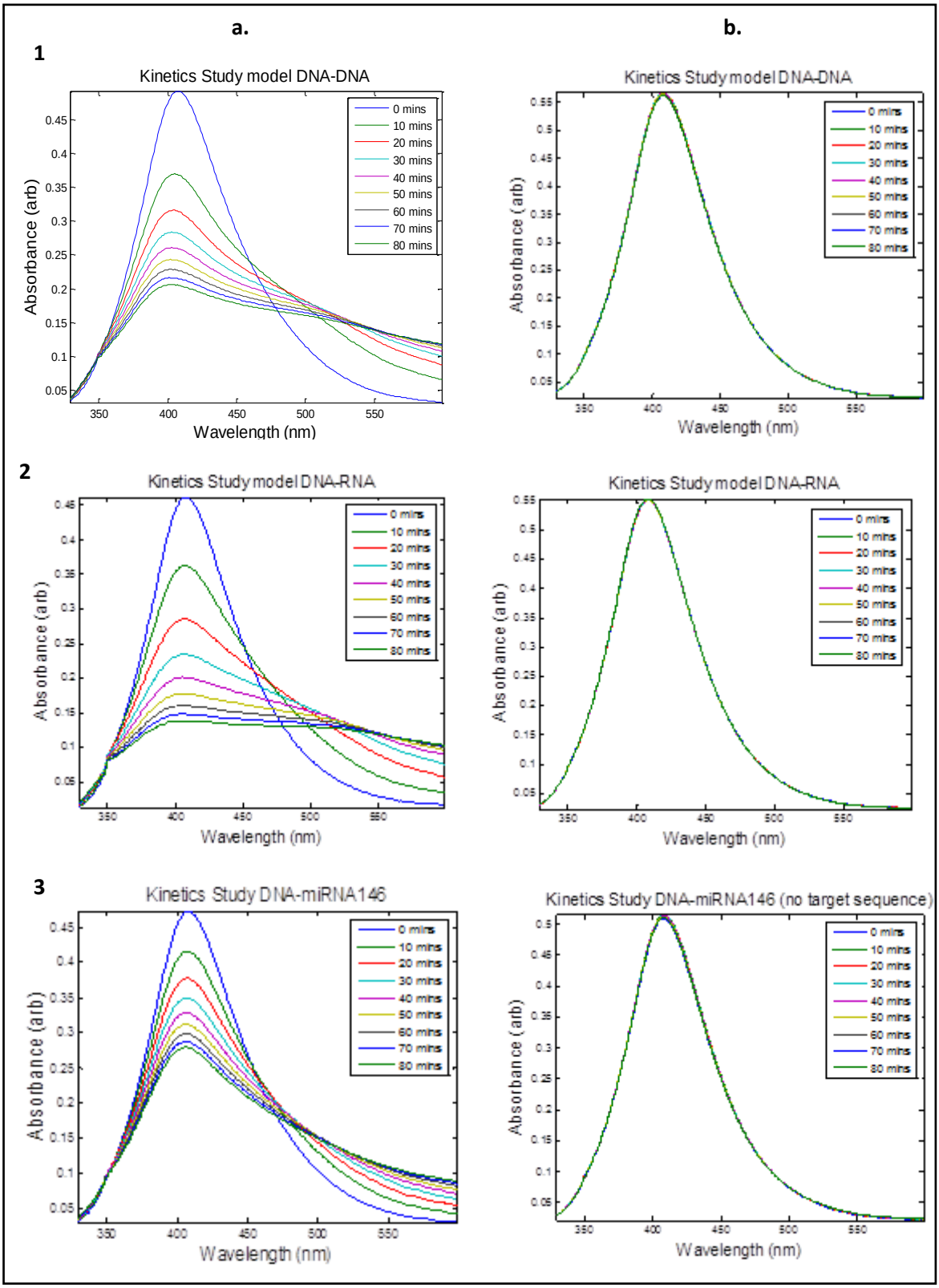
a.
b.
1
Kinetics Study model DNA-DNA
Absorbance (arb)
Wavelength (nm)
0 mins
10 mins
20 mins
30 mins
40 mins
50 mins
60 mins
70 mins
80 mins
Kinetics Study model DNA-DNA
Absorbance (arb)
Wavelength (nm)
2
Kinetics Study model DNA-RNA
Absorbance (arb)
Wavelength (nm)
Kinetics Study model DNA-RNA
Absorbance (arb)
Wavelength (nm)
3
Kinetics Study DNA-miRNA146
Absorbance (arb)
Wavelength (nm)
Kinetics Study DNA-miRNA146 (no target sequence)
Absorbance (arb)
Wavelength (nm)

Figure 4.4. Extinction spectra showing kinetic time studies. Column **a.** represents samples where a target sequence was present. Column **b**. represents samples where a nonsense or no sequence was present. Rows; 1: DNA-DNA, 2: DNA-RNA, 3: DNA-miRNA146a.

From visual inspection, the first obvious observation is the distinct difference in spectra when a target sequence is present to when a nonsense sequence is present. In the latter cases, no change in absorbance is observed, suggesting that no change in particle size, shape or concentration occurs during the period of study. Thus suggesting no aggregation and hence no hybridisation has occurred. Conversely, when a target sequence is present, a clear pattern in maximum absorbance values is observed. In all three cases, the rate of hybridisation followed an inverse exponential rate. All three duplexes; DNA-DNA, DNA-RNA and DNA-miRNA had an initial λ_{max} absorbance value just below 0.5 a.u. The DNA-RNA duplex hybridised the quickest with the greatest decrease in maximum absorbance value, i.e. plateau was reached first. DNA-DNA also hybridised quickly with a final absorbance value just higher than that of the RNA duplex. The DNA-miRNA duplex hybridised the slowest with the final absorbance value lying at a much higher value than the other duplexes. This shows that for DNA-miRNA duplexes, a longer period of time is required for the same state of aggregation to be achieved as for DNA-DNA/RNA. Further studies are required to show if this is the case for all DNA-miRNA duplexes. In all three cases, a longer time period was required for full hybridisation (plateau) to be reached.

4.2.5. Hybridisation Vs Time Study

Hybridisation time studies were performed to compare the rate of hybridisation of the different duplexes with respect to time. The data was interpreted by following the peak area of the 1172 cm^{-1} peak representative of malachite green. The greater the peak area, the greater the spectral feature hence the greater the malachite green signal suggesting a higher degree of aggregation thus hybridisation. The spectral data was baseline corrected prior to peak area calculation. DNA-DNA and DNA-RNA followed a similar pattern as seen in Figure 4.5. Both duplexes displayed an exponential curve. (The initial rate of hybridisation was high and decreased each time step until a plateau was reached at which point no further hybridisation occurred).

DNA-MiRNA showed a similar shape however a plateau was not reached. This may be due to the time period studied. Had a longer period of time been observed, it would be expected to have followed the same deceleration curve as the DNA and RNA duplexes.

By observing the shape of the hybridisation curves it is clear that DNA-DNA and DNA-RNA duplexes hybridise at a similar rate whilst DNA-miRNA takes a longer period of time to fully hybridise.

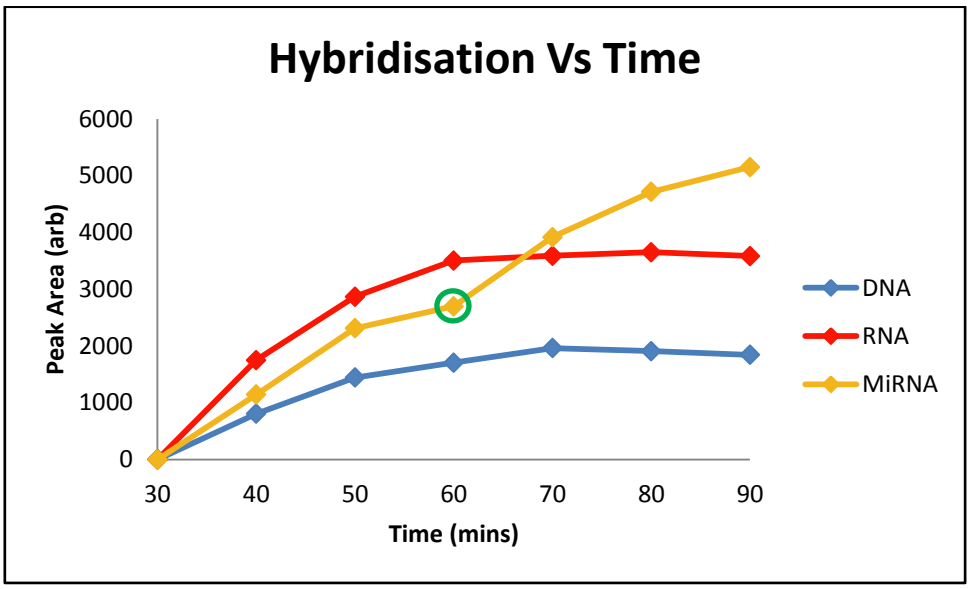

Figure 4.5. Hybridisation Vs Time graph for DNA-DNA, DNA-RNA and DNA-miRNA duplexes. Figure displays peak area of baseline corrected 1172 cm^{-1} peak plotted against time. Highlighted MiRNA data point at 60 minutes is an outlier.

4.2.6. Serum Doping

When the appropriate probe-target and hybridisation conditions were chosen and optimised from the above experiments, the next stage was to better mimic a real life sample whereby miRNA detection for CVD would occur. The ultimate aim of this section of the project is to extract, detect and identify CVD related miRNA's from blood samples. The miRNA's relevant for these purposes are circulating miRNA's present in blood, specifically serum. To mock this, synthetic serum was purchased and doped into the hybridisation samples.

A series of doping experiments were performed by varying the composition of PBS and synthetic serum in the hybridisation medium. The control was 100 % PBS as per the standard hybridisation procedure. When 100 % PBS was used, the resulting spectra displayed a clear and defined signal with minimal background. From this, a clear ON:OFF signal could be seen and thus the presence of a target sequence could be determined.

When synthetic serum was added an immediate background was observed. This was the case for all the dilutions of PBS and serum mixtures. A number of repeats were performed and in all cases, a background was observed. From this it was concluded that the presence of serum, independent of

the amount, caused a high background to be present. The presence of the background caused the relative intensities of the spectra to be obscured and consequently by visual inspection of the spectra, an ON:OFF signal could not be observed. However, further processing of the data allowed masked data to be extracted. Unique peaks corresponding to the Raman reporter were selected (1172 cm^{-1} and 1618 cm^{-1}). The corresponding spectral data was baseline corrected and the peak areas calculated. Comparison of the peak areas allowed discrimination between target presence/absence to be seen. An example set of dilution series spectra and the calculated peak areas for the 1172 cm^{-1} peak is displayed in Figure 4.6. As can be seen, there is an obvious difference in the peak area of samples where a target sequence is present and those when it is not. This thereby provides a comparable parameter able of deducing the presence or absence of a target sequence in the presence of serum.

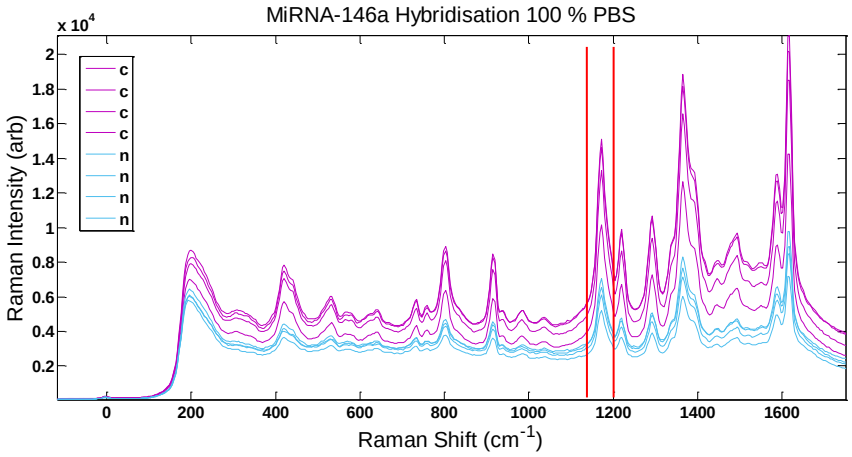
MiRNA-146a Hybridisation 100 % PBS
x 10^4
Raman Intensity (arb)
Raman Shift (cm^-1)
c
c
c
c
n
n
n
n

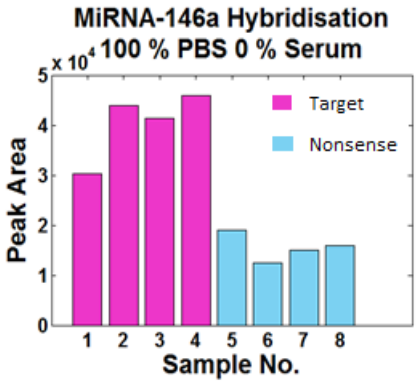
MiRNA-146a Hybridisation
100 % PBS 0 % Serum
x 10^4
Peak Area
Target
Nonsense
Sample No.

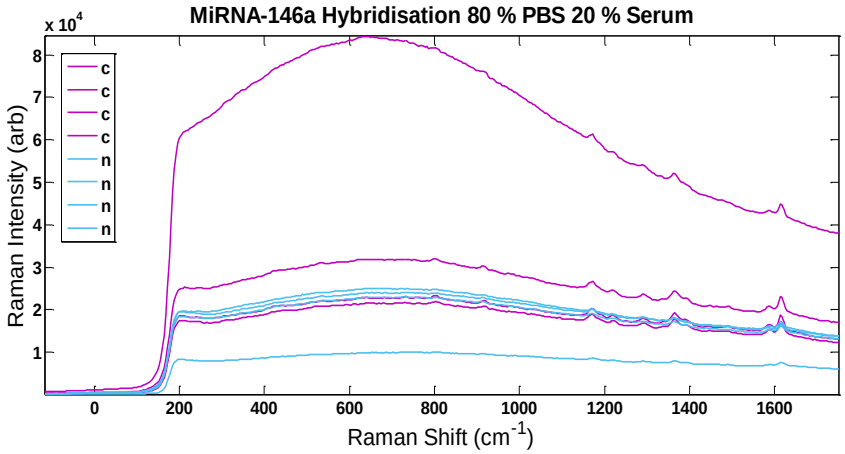
MiRNA-146a Hybridisation 80 % PBS 20 % Serum
x 10^4
Raman Intensity (arb)
Raman Shift (cm^-1)
c
c
c
c
n
n
n
n

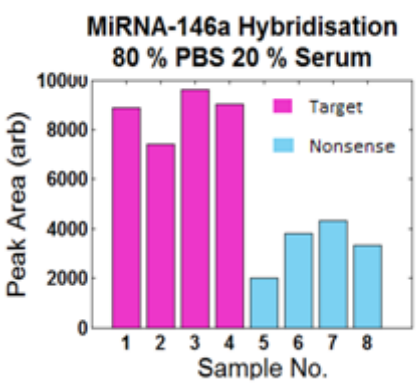
MiRNA-146a Hybridisation
80 % PBS 20 % Serum
Peak Area (arb)
Target
Nonsense
Sample No.

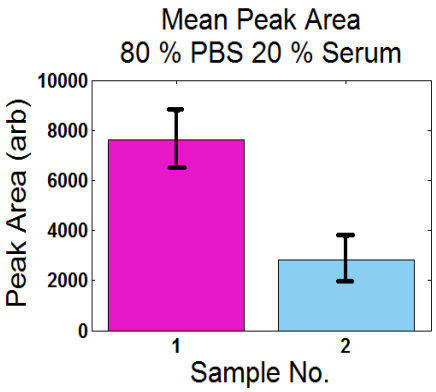
Mean Peak Area
80 % PBS 20 % Serum
Peak Area (arb)
Sample No.

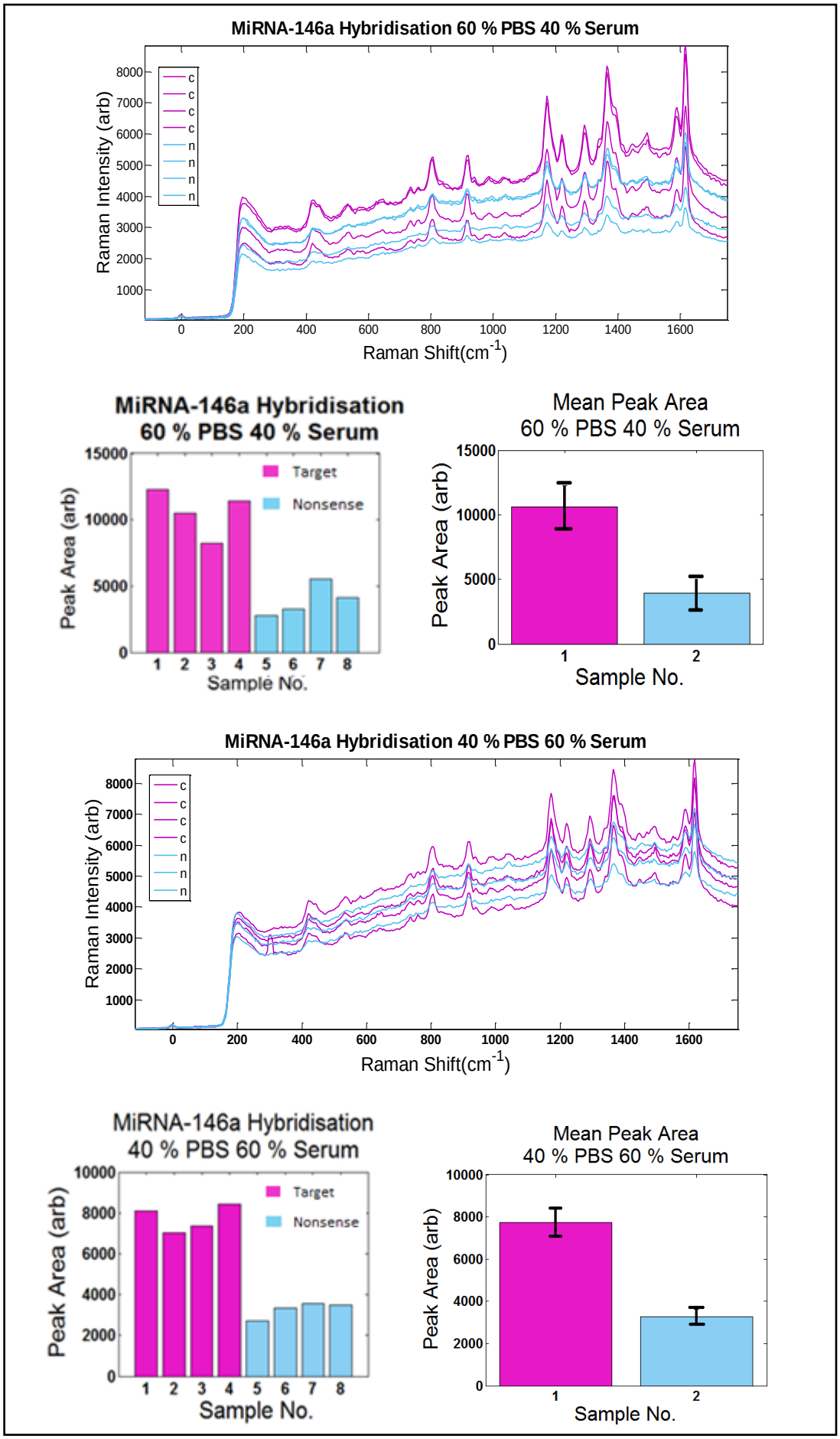
MiRNA-146a Hybridisation 60 % PBS 40 % Serum
Raman Intensity (arb)
Raman Shift(cm-1)
c
c
c
c
n
n
n
n
MiRNA-146a Hybridisation
60 % PBS 40 % Serum
Peak Area (arb)
Target
Nonsense
Sample No.
Mean Peak Area
60 % PBS 40 % Serum
Peak Area (arb)
Sample No.
MiRNA-146a Hybridisation 40 % PBS 60 % Serum
Raman Intensity (arb)
Raman Shift(cm-1)
MiRNA-146a Hybridisation
40 % PBS 60 % Serum
Peak Area (arb)
Target
Nonsense
Sample No.
Mean Peak Area
40 % PBS 60 % Serum
Peak Area (arb)
Sample No.

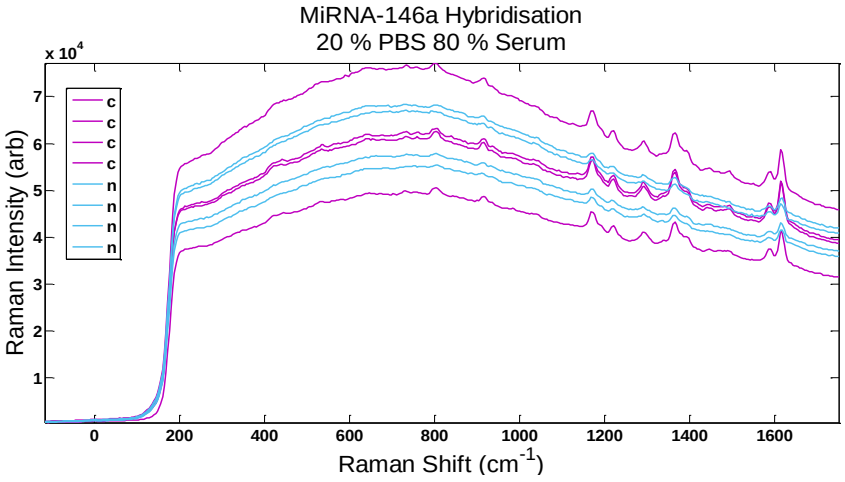
MiRNA-146a Hybridisation
20 % PBS 80 % Serum
x 10^4
Raman Intensity (arb)
c
c
c
c
n
n
n
n
Raman Shift (cm^-1)

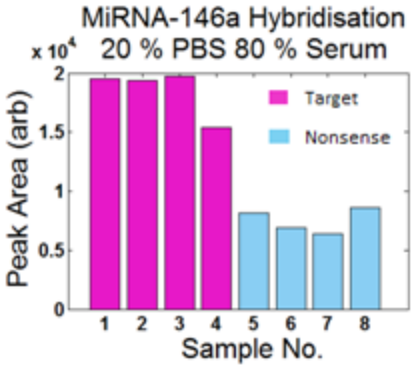
MiRNA-146a Hybridisation
20 % PBS 80 % Serum
x 10^4
Peak Area (arb)
Target
Nonsense
Sample No.

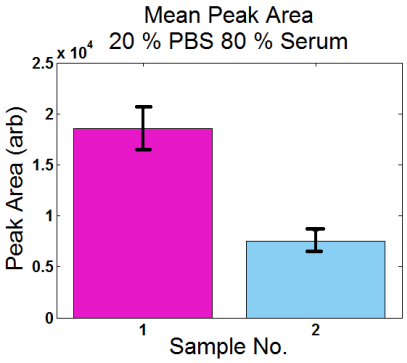
Mean Peak Area
20 % PBS 80 % Serum
x 10^4
Peak Area (arb)
Sample No.

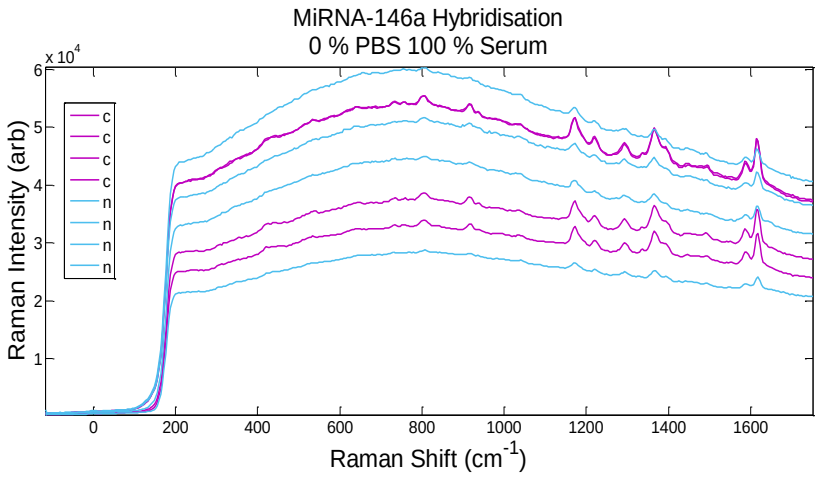
MiRNA-146a Hybridisation
0 % PBS 100 % Serum
x 10^4
Raman Intensity (arb)
c
c
c
c
n
n
n
n
Raman Shift (cm^-1)

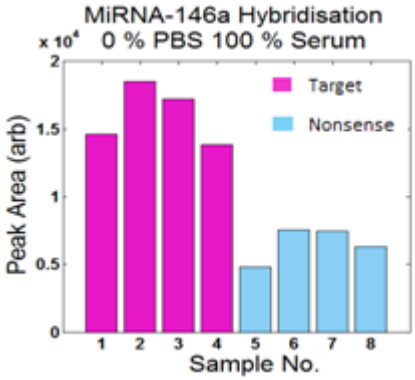
MiRNA-146a Hybridisation
0 % PBS 100 % Serum
x 10^4
Peak Area (arb)
Target
Nonsense
Sample No.

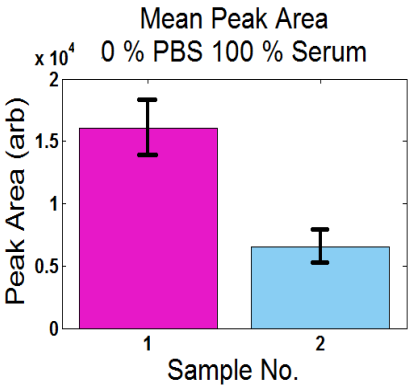
Mean Peak Area
0 % PBS 100 % Serum
x 10^4
Peak Area (arb)
Sample No.

Figure 4.6. Serum doping data for **a.** 100 % PBS, **b.** 80 % PBS 20 % serum, **c.** 60 % PBS 40 % serum, **d.** 40 %PBS 60 % serum, **e.** 20 % PBS 80 % serum and **f.** 100 % serum each showing **i.** Raw Raman spectra, **ii.** Peak area for baseline corrected 1172 cm^{-1} peak and **iii.** Mean peak area.

Since synthetic serum is the closest mimic to true serum, the ability to correctly identify the presence of target miRNA in synthetic serum is promising for the use of the assay in real serum samples.

4.3. Cholesterol Covered Nanoparticles

The aim of this synthesis was to prepare nanoparticles capable of cell layer penetration. There are two main mechanisms by which a particle can pass through a membrane; passive or active transport [76]. Passive transport obeys the second law of thermodynamics whereby molecules will pass through a membrane from a high concentration to a region of lower concentration in order to increase the entropy of the cell. This process is concentration, size and charge dependent. Active transport is when energy is required to move molecules from one side of the membrane to the other. This is usually due to movement against a concentration gradient.

For the purposes of this study, passive transport is the movement of interest. However, in order for particles to move across the phospholipid cell bilayer, they must be able to dissolve in the bilayer and thus must possess lipophilic properties [77]. A variety of functionalities may be suitable for such purposes. Cholesterol is a naturally occurring lipid modified steroid synthesised in animal cells. The properties of cholesterol are desirable for membrane transport. Cholesterol can be easily conjugated to an oligonucleotide and as previously demonstrated. Oligonucleotides can be easily conjugated to a nanoparticle. Also, due to its natural occurrence, it was expected to have good stability in a biological environment and as a result, was the functionality of choice.

4.3.1. Synthesis

For the initial set of experiments 100 % cholesterol covered nanoparticles in water were used. When 100 % cholesterol coverage was performed, attempts to resuspend in PBS caused the particles to crash out. Thus in order for further analysis to be carried out, resuspension in water was necessary.

When suspended in water and a negatively charged dye added at 2500 dye molecules per nanoparticle, the particles also crashed out. It was therefore implied that the stability of 100 % cholesterol covered particles was poor in charged solutions.

As stability is an integral component of these particles and the ultimate aim is for use in a biological environment, it was essential that they were stable in a charged environment. The solution to this was to create a mixed monolayer consisting of a model probe sequence and the oligo-cholesterol sequence. This was performed as 100 % model probe covered nanoparticles are stable in PBS as shown in the first section of this report, thus suggesting that mixing them with the unstable cholesterol moiety may initiate stability.

4.3.2. Characterisation

Various spin speeds and times were performed during the synthesis of cholesterol covered particles, yet the optimum parameters that inferred the cholesterol covered particles were being recovered were 5000 rpm for 20 minutes.

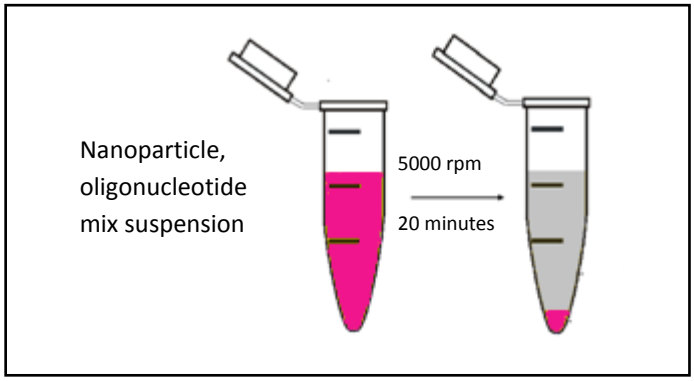

Figure 4.7. Schematic showing cholesterol covered particle synthesis.

4.3.2.1. Extinction Spectroscopy and Nanosizer Analysis

Initially, 100 % cholesterol covered particles were synthesised. When attempts were made to resuspend the pellet in 0.1 M PBS, the particles aggregated visualised by a colour change of pink to a dark purple. This was further confirmed by DLS analysis which showed the average diameter of the PBS suspended particles to have drastically increased. However, when resuspended in water, the particles remained stable. A change in λ_{max} and size was observed when compared to unfunctionalized nanoparticles, suggesting a change in surface properties (i.e. addition of cholesterol).

In order to overcome the lack of stability of the particles in salt solution, mixed monolayer samples were prepared. The Extinction and DLS data for the mixed monolayer covered particles is shown in Tables 4.1. and 4.2.

Sample	λ_{max} (nm)
Bare nanoparticle	521
Conjugated nanoparticles	525

Table 4.1. Extinction spectra data for cholesterol covered particles.

Coverage Composition		Average Size (nm)	Average SD (nm)
% model probe	% oligo-cholesterol		
Bare nanoparticles		20.45	0.563
100	0	25.83	0.541
50	50	27.94	0.516
0	100	42.50	0.482

Table 4.2. DLS data for cholesterol covered particles of varying compositions.

The first important finding during the synthesis of the mixed monolayer particles was that when resuspended in 0.1 M PBS they remained stable. This enabled progression with further studies.
As seen from the extinction data, there is a shift in the λ_{max} position from bare nanoparticles to conjugated particles. The shift observed displays a higher wavelength after conjugation, this is known as a red shift. The λ_{max} is the wavelength at which the highest absorbance occurs. In relation to nanoparticles, this value changes with the size of particle and/or surface functionality. Hence, the shifts observed in these experiments suggest a change in surface properties from the bare nanoparticles to the conjugated nanoparticles.

The DLS data also displays a change when the different compositions of model probe and cholesterol is added. The instrument used measures the average diameter of particles via dynamic light scattering (DLS) measurements. Briefly, the sample is exposed to light which is scattered by the particles in all directions. This scattering fluctuates due to Brownian motion of the particles. Constructive and destructive interference from neighbouring particles occurs and from this, information on the time scale of movement and consequently size of particles can be deduced.

The average size of particle increased when bare nanoparticles were functionalised with model probe sequence. The particle size further increased when 50:50 probe:cholesterol mix was added to the surface. Particles with 100 % cholesterol coverage displayed the greatest particle size. The increase in size from bare nanoparticles to model probe covered particles to cholesterol covered particles is as expected. The conjugation of oligonucleotides to the nanoparticle surface adds an

extra layer to the particle thus increases its size. Furthermore, the oligo-cholesterol moiety has a larger molecular size than the model probe oligonucleotide and thus upon incorporation onto the surface further increases the particle size.

This pattern was consistent with a number of repeats.

4.3.2.2. Gel Electrophoresis

Gel electrophoresis was used to separate the particles according to size and charge. The gel is set up so that the negative electrode is at the well end and the positive electrode is at the bottom end of the gel. The nanoparticles possess an overall negative charge and thus migrate towards the positive end of the gel. As the particles migrate down the gel, the smallest particles will travel the fastest whilst the larger particles will move at a slower speed thereby separating the particles according to size. Since the cholesterol covered nanoparticles should have a larger diameter due to the larger molecular size of cholesterol compared to lone oligonucleotides, the cholesterol covered particles should travel less distance than the model probe covered particles.

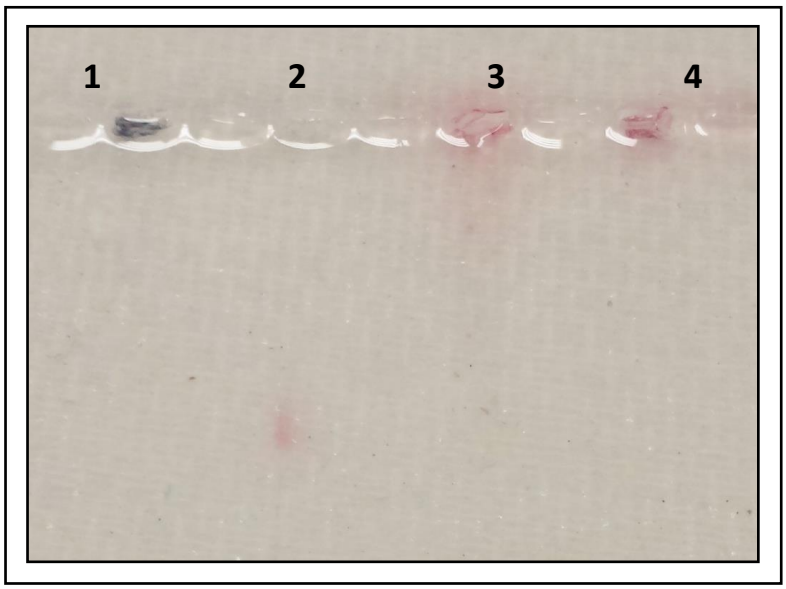

Figure 4.8. 1 % agarose gel ran at 165 V Well 1: bare nanoparticles 2: 100 % model probe3: 50:50 % model : cholesterol 4: 100 % cholesterol

As seen in Figure 4.8., when bare nanoparticles were placed into the buffered well, they instantly crashed out. This is due to the destabilising effect the addition of the loading buffer (SYBR green) has on the bare nanoparticles. As there is no protecting barrier in the form of an oligonucleotide layer on the bare nanoparticles, when SYBR green is added, it attaches to the nanoparticle surface via thiol affinity. The positive charge the molecule possesses has an overall neutralising effect on the negatively charged nanoparticles. This therefore allows the particles to move within close proximity of each other and aggregate.

Well 2 represents 100 % model probe covered nanoparticles and the third well represents 50:50 mixed monolayer covered nanoparticles. These particles remained in suspension due to the protecting layer the oligonucleotides create on the nanoparticle surface. By comparison, the pure model probe nanoparticles migrated much further down the gel in a single band. The mixed monolayer sample displayed a gradual migration of particles down the gel. This suggested that the mixed monolayer particles were of variable sizes whilst the model probe particles were consistent in size. One reason for the dispersion of mixed monolayer particles may be that the functionalisation of nanoparticles with the oligonucleotide mix is not consistent. Various factors may affect this such as rate of movement in solution. These results are consistent with the larger molecular size of the cholesterol moiety compared to the model probe sequence.

The final well represents 100 % cholesterol covered nanoparticles. These particles remained in suspension yet no migration was observed. By visual observation, the colour appears to have darkened suggesting a degree of aggregation, which would consequently result in larger particle sizes and thus migration may be too slow to observe in the time period the gel was ran. This aggregation may be as a result of the addition of the positively charged loading buffer as earlier experiments displayed the lack of stability of 100 % cholesterol covered particles in charged solutions.

In addition to the above explanation for the gel electrophoresis observations, another contribution may be due to the addition of the cholesterol compound. It is possible that it altered the overall charge contribution from the DNA, making it less significant. A lower net charge would result in a weaker attraction of the particles to the end of the gel and thus travel at a slower rate.

4.3.3. Biological Activity of Cholesterol Covered Nanoparticles

Following on from the synthesis of the cholesterol covered nanoparticles, the next stage was to determine their biological activity. This was performed by investigating the interaction between the particles and cells.

The first experiment performed was to check the stability of the particles in cell media. This was performed by spinning down the particles and resuspending the pellet in cell media. Three samples; 100 % model probe, 50:50 % mixed monolayer and 100 % cholesterol covered particles were tested. The 100 % model probe and 50:50 mixed monolayer covered particles remained disperse in solution. The 100 % cholesterol covered particles slightly aggregated over a period of time, evident by a resulting darker colour. Since the 50:50 mixed monolayer particles were stable in media, these were the particles used for further experimentation.

Next, incubation of the particles in macrophage cells was performed. This was carried out in an attempt to see whether or not the particles could be inserted into the cells (i.e. could pass through the phospholipid bilayer). Three controls were performed in which cells were incubated with; bare nanoparticles, 50:50 mixed monolayer covered particles and no nanoparticles. The results are displayed in Figure 4.9.

a-f in Figure 4.9. display white light images of cells, whilst i-vi display the colour intensity spectral maps of the corresponding white light images. Maps were generated using a devised code in Matlab. The code was designed to generate a map from the spectral matrix by selecting data corresponding to a specific peak, baseline correcting to remove any background and calculating the resulting peak area which was subsequently used to produce a colour intensity map. Baseline correction of each individual spectrum was performed prior to peak area calculation in an attempt to remove any interference from variable background signals around the cell and thus remove the chance of a false colour image of background being produced. All parameters for the maps remained constant to allow for comparison of the different samples.

The different colour intensities of the spectral maps correspond to the value of peak area of the 1172 cm^{-1} peak. As the scale moves from blue to red, the peak area increases which corresponds to the signal intensity for malachite green. A malachite green signal indicates the presence of nanoparticles to which the Raman reporter is attached, thus by deducing a map of the signal, the location of the nanoparticles can be seen.

As shown by the control maps where no Raman reporter molecules were present, the cell cannot be visualised. This is due to no corresponding peaks present. The maps generated for the cells incubated with 50:50 mixed monolayer functionalised nanoparticles with Raman reporter displayed clear areas in which the signal was high, representing the presence of malachite green. These areas of high intensity mimicked the areas in which cells were present in the white light images. Furthermore, the outline of the cells could also be made out in a number of the spectral maps. Areas in these maps where no cell was present possessed a dark blue colour indicating no spectral feature thereby no malachite green presence.

These results displaying the present of malachite green signal in the areas of cell presence and the lack of signal where cells are not present, strongly suggest that the particles are being taken up by the cells.

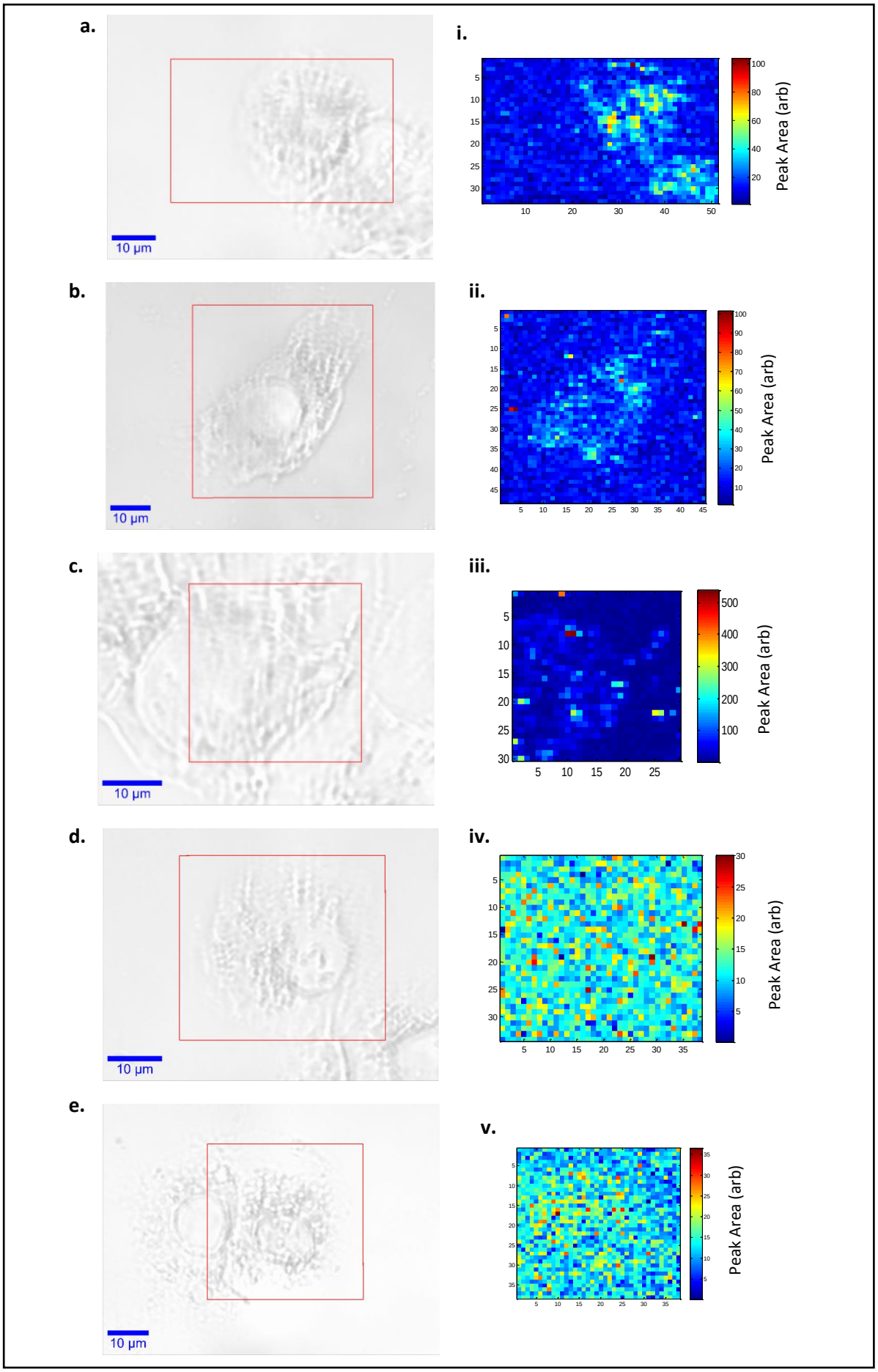
a.
10 µm
i.
Peak Area (arb)
b.
10 µm
ii.
Peak Area (arb)
c.
10 µm
iii.
Peak Area (arb)
d.
10 µm
iv.
Peak Area (arb)
e.
10 µm
v.
Peak Area (arb)

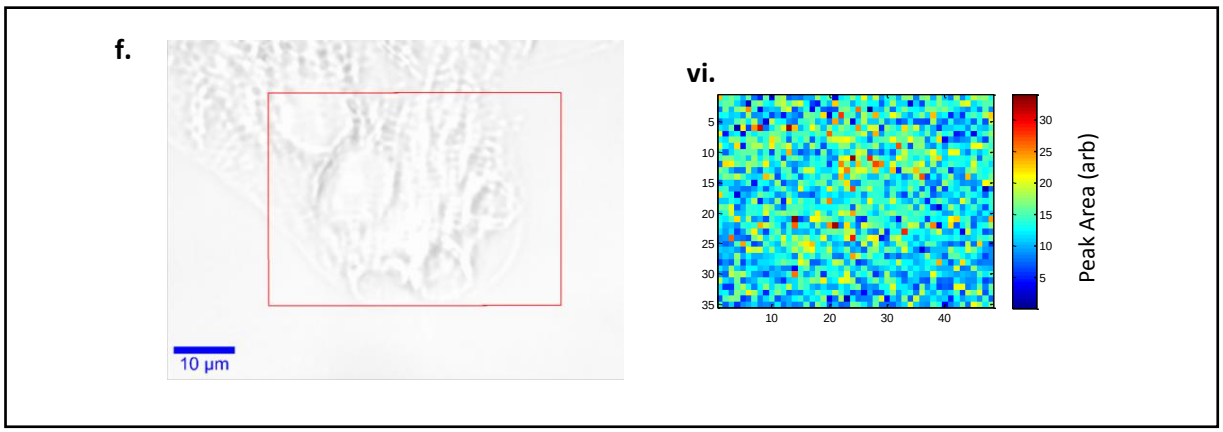

Figure 4.9. a.-f. 50x white light images of cells displaying mapped area encased by red box. The images represent cells incubated with **(a-c.)** 50:50 mixed monolayer covered nanoparticles functionalised with malachite green, **(d.)** 50:50 mixed monolayer covered nanoparticles (no malachite green), **(e.)** bare nanoparticle and **(f.)** no nanoparticles (bare cells). **i.-vi.** Spectral maps of corresponding white light images. Spectral maps created on a colour intensity scale from the value of the baseline corrected peak area of the 1172 cm^{-1} peak.

5. Conclusions

The first aim of this project was to create an assay capable of miRNA detection. By preparing nanoparticle oligonucleotide conjugates using the fast conjugate synthesis with sequence specific DNA, nanoparticle probes were created which could then be used to detect the presence of a target miRNA sequence. By functionalising the nanoparticle probes with a Raman reporter, this allowed a unique signal to be produced when analysed via Raman spectroscopy. In the presence of a target sequence, complementary base pairing occurs between the probes and target sequence which results in the aggregation of the nanoparticles. This in turn causes an increase in the Raman signal due to coupling of the surface plasmons and subsequent formation of optical hotspots. This thereby provides a characteristic feature by which the presence of a target sequence can be identified.

The use of synthetic serum in hybridisation experiments allowed the assay to better mimic the conditions of a real life sample whereby miRNA detection would occur. The results obtained from these experiments showed that although the presence of serum obstructed the visual interpretation of the Raman spectra, with further data processing, an ON:OFF SERS signal could be achieved and thus the presence or absence of a target sequence could be deduced. This shows potential for the use of the assay in real life serum samples.

The second aim of this project was to create nanoparticles capable of cell layer penetration. This was performed by coating nanoparticles in a layer of cholesterol. The cholesterol was added to the surface by conjugating a cholesterol TEG structure to the 3’ end of a twelve base oligonucleotide, of which the 5’ end was modified with a thiol. The thiol enabled the attachment of the cholesterol oligonucleotide moiety to the surface of the nanoparticle. In order to maintain stability of the particles in buffered solutions, a mixed monolayer of cholesterol and model probes oligonucleotide sequences was required.

The prepared particles were then incubated in macrophage cells and mapped using Raman spectroscopy. The data was processed using a self programmed code in Matlab in order to remove any background interference from the cell. The results from these experiments enabled visualisation of the cells in the spectral maps due to the presence of a malachite green signal. Areas where there were no cells displayed no signal. Since malachite green was only present on the functionalised nanoparticle surface, this suggests that the particles had inserted into the cells.

6. Future Work

A successful assay capable of the detection of miRNA was produced in this project. The next stage will be to multiplex the assay to enable the simultaneous detection of multiple miRNA sequences linked to CVD. The ability to quantify the amount of miRNA present in a sample should also be attempted. It would also be useful to perform a limit of detection study to establish the limit of which miRNA detection can occur.

Once a successful multiplex assay is developed, it may be used for clinical samples of predetermined stages of atherosclerosis. MiRNA extraction and detection of sequences could be performed in an attempt to establish any miRNA biomarkers (either upregulated or downregulated) related to the presence of atherosclerosis. Once biomarkers have been identified, attempts to quantify levels of such sequences in the predetermined samples could be performed in order to establish any links between levels of circulating miRNA and stage of the disease.

The next stage in the experimentation on cholesterol covered nanoparticles could be to access the interaction of the particles with different cell lines in order to see if they interact in the same way as with the macrophages. The cell lines used should be those relevant to atherosclerotic plaques. Further to this, a synthetic atherosclerotic plaque could be used. The plaque should be structurally designed to mimic the cell layers present in a real life plaque. The aim of this would be to apply the particles to the top layer of cells and for the particles to penetrate through the layers to the bottom macrophage layer.

Once cell layer penetration is successful, the utilisation of hollow gold nanoshells in place of the solid gold particles should be performed. The reason for this would be to investigate their potential use as a drug delivery agent, specific for the treatment of atherosclerosis.

7. References

1. Schrader, B., *Infrared and Raman spectroscopy: methods and applications*. 2008: John Wiley & Sons.
2. Smith, E. and Dent, G., *Modern Raman spectroscopy: a practical approach*. 2005: John Wiley & Sons.
3. Albani, J.R., *Principles and Applications of Fluorescence Spectroscopy*. 2007: Blackwell.
4. Zare, R.N., *Laser Experiments for Beginners*. 1995: University Science Books.
5. Valeur, B. and Berberan-Santos, M.N., *Molecular Fluorescence: Principles and Applications*. 2013: Wiley.
6. [cited 2014 02/02/2014]; Available from: http://chemwiki.ucdavis.edu/Physical_Chemistry/Spectroscopy/Electronic_Spectroscopy/Jablonski_diagram.
7. Bailo, E. and Deckert, V., *Tip-enhanced Raman scattering.* Chemical Society Reviews, 2008. **37**(5): p. 921-930.
8. Campion, A. and Kambhampati, P., *Surface-enhanced Raman scattering.* Chemical Society Reviews, 1998. **27**(4): p. 241-250.
9. Kneipp, K., Moskovits, M., and Kneipp, H., *Surface-enhanced Raman scattering: physics and applications*. Vol. 103. 2006: Springer.
10. Fleischmann, M., Hendra, P.J., and McQuillan, A.J., *Raman spectra of pyridine adsorbed at a silver electrode.* Chemical Physics Letters, 1974. **26**(2): p. 163-166.
11. Nie, S. and Emory, S.R., *Probing Single Molecules and Single Nanoparticles by Surface-Enhanced Raman Scattering.* Science, 1997. **275**(5303): p. 1102-1106.
12. Albrecht, M.G. and Creighton, J.A., *Anomalously intense Raman spectra of pyridine at a silver electrode.* Journal of the American Chemical Society, 1977. **99**(15): p. 5215-5217.
13. Ringe, E., et al., *Single nanoparticle plasmonics.* Physical Chemistry Chemical Physics, 2013. **15**(12): p. 4110-4129.
14. McQuillan, A.J., *The discovery of surface-enhanced Raman scattering.* Notes and Records of the Royal Society, 2009. **63**(1): p. 105-109.
15. Association, A.H. *Heart Disease Fact Sheet*. 2015.
16. Foundation, B.H. *Heart Statistics*. 2015 13.02.15 [cited 2015 10.06.15]; Available from: https://www.bhf.org.uk/research/heart-statistics.
17. Mendis, S., Puska, P., and Norrving, B., *Global Atlas on Cardiovascular Disease Prevention and Control*. 1 ed, ed. Shanthi Mendis, Pekka Puska, and B. Norrving. 2011, www.who.int: World Health Organisation.
18. Toth, P.P., *Subclinical atherosclerosis: what it is, what it means and what we can do about it.* International Journal of Clinical Practice, 2008. **62**(8): p. 1246-1254.
19. Sanchez Santana, M.A. et al. *A Tool for Telediagnosis of Cardiovascular Disease in a Collaborative and Adaptive Approach.* J Univers Comput Sci, 2013. **19**(9)
20. Libby, P., Ridker, P.M., and Hansson, G.K., *Progress and challenges in translating the biology of atherosclerosis.* Nature, 2011. **473**(7347): p. 317-325.
21. Glagov, S., et al., *Compensatory Enlargement of Human Atherosclerotic Coronary Arteries.* New England Journal of Medicine, 1987. **316**(22): p. 1371-1375.
22. Anderson, J.D. and Kramer, C.M., *MRI of Atherosclerosis: Diagnosis and Monitoring Therapy.* Expert review of cardiovascular therapy, 2007. **5**(1): p. 69-80.
23. Insull Jr, W., *The Pathology of Atherosclerosis: Plaque Development and Plaque Responses to Medical Treatment.* The American Journal of Medicine, 2009. **122**(1, Supplement): p. S3-S14.
24. Kawasaki, E.S. and Player, A., *Nanotechnology, nanomedicine, and the development of new, effective therapies for cancer.* Nanomedicine: Nanotechnology, Biology and Medicine, 2005. **1**(2): p. 101-109.

25. Morrow Jr, K.J., Bawa, R., and Wei, C., *Recent Advances in Basic and Clinical Nanomedicine.* Medical Clinics of North America, 2007. **91**(5): p. 805-843.
26. Catherine, C.B. and Adam, S.G.C., *Functionalisation of magnetic nanoparticles for applications in biomedicine.* Journal of Physics D: Applied Physics, 2003. **36**(13): p. R198.
27. Gracie, K., et al., *Simultaneous detection and quantification of three bacterial meningitis pathogens by SERS.* Chemical Science, 2014. **5**(3): p. 1030-1040.
28. Hahm, J.-i. and Lieber, C.M., *Direct Ultrasensitive Electrical Detection of DNA and DNA Sequence Variations Using Nanowire Nanosensors.* Nano Letters, 2004. **4**(1): p. 51-54.
29. De Jong, W.H. and Borm, P.J.A., *Drug delivery and nanoparticles: Applications and hazards.* International Journal of Nanomedicine, 2008. **3**(2): p. 133-149.
30. Auffan, M., et al., *Towards a definition of inorganic nanoparticles from an environmental, health and safety perspective.* Nat Nano, 2009. **4**(10): p. 634-641.
31. Buzea, C., Pacheco, I., and Robbie, K., *Nanomaterials and nanoparticles: Sources and toxicity.* Biointerphases, 2007. **2**(4): p. MR17-MR71.
32. Tweney, R.D., *Discovering discovery: How faraday found the first metallic colloid.* Perspectives on Science, 2006. **14**(1): p. 97-121.
33. Ashby, M.F.F.P.J.S.G.S.D.L. *Nanomaterials, nanotechnologies and design an introduction for engineers and architects*. Amsterdam: Butterworth-Heinemann/Elsevier.
34. Bobo, D., Robinson, K.J., Islam, J. et al. *Nanoparticle-Based Medicines: A Review of FDA-Approved Materials and Clinical Trials to Date*. Pharm Res, 2016 33(10): p2373-2387
35. Ghosh, S.K. and Pal, T., *Interparticle Coupling Effect on the Surface Plasmon Resonance of Gold Nanoparticles: From Theory to Applications.* Chemical Reviews, 2007. **107**(11): p. 4797-4862.
36. Craig, D., et al., *Formation of SERS active nanoparticle assemblies via specific carbohydrate-protein interactions.* Chemical Communications, 2013. **49**(1): p. 30-32.
37. Barrett, L., et al., *Stable dye-labelled oligonucleotide-nanoparticle conjugates for nucleic acid detection.* Nanoscale, 2011. **3**(8): p. 3221-3227.
38. Jamdagni, P., Khatri, P. and Rana, J.S. *Nanoparticles based DNA conjugates for detection of pathogenic microorganisms.* Int Nano Lett. 2016 **6**(3) p: 139–146
39. Hakkinen, H., *The gold-sulfur interface at the nanoscale.* Nat Chem, 2012. **4**(6): p. 443-455.
40. Chen, X.J. et al. *Noble metal nanoparticles in DNA detection and delivery*. WIREs Nanomed Nanobiotechnol. 2012 **4**(3) p: 273-90
41. Cao, Y.C., Jin, R. and Mirkin, C.A. *Nanoparticles with Raman Spectroscopic Fingerprints for DNA and RNA Detection.* Science. 2002: **297**(5586) p: 1536-4
42. Thompson, D., Faulds, K, Smith, E.W. and Graham, D. *Precise Control of the Assembly of Dye-Coded Oligonucleotide Silver Nanoparticle Conjugates with Single Base Mismatch Discrimination Using Surface Enhanced Resonance Raman Scattering.* J. Phys. Chem. *C*, 2010, ***114***(16) p: 7384–7389
43. MacAskill, A., Crawford, D., Graham, D. and Faulds, K. *DNA Sequence Detection Using Surface-Enhanced Resonance Raman Spectroscopy in a Homogeneous Multiplexed Assay*. *Anal. Chem.* **81**(19) p: 8134-8140
44. Liu, Y. and Huang, C.Z., *One-step conjugation chemistry of DNA with highly scattered silver nanoparticles for sandwich detection of DNA.* Analyst, 2012. **137**(15): p. 3434-3436.
45. Lee, R.C., Feinbaum, R.L., and Ambros, V., *The C. elegans heterochronic gene lin-4 encodes small RNAs with antisense complementarity to lin-14.* Cell, 1993. **75**(5): p. 843-854.
46. Reinhart, B.J., et al., *The 21-nucleotide let-7 RNA regulates developmental timing in Caenorhabditis elegans.* Nature, 2000. **403**(6772): p. 901-906.
47. Pasquinelli, A.E., et al., *Conservation of the sequence and temporal expression of let-7 heterochronic regulatory RNA.* Nature, 2000. **408**(6808): p. 86-89.

48. Madrigal-Matute, J., et al., *MicroRNAs and Atherosclerosis.* Current Atherosclerosis Reports, 2013. **15**(5): p. 1-8.
49. Mitchell, P.S., et al., *Circulating microRNAs as stable blood-based markers for cancer detection.* Proceedings of the National Academy of Sciences of the United States of America, 2008. **105**(30): p. 10513-10518.
50. Valadi, H., et al., *Exosome-mediated transfer of mRNAs and microRNAs is a novel mechanism of genetic exchange between cells.* Nat Cell Biol, 2007. **9**(6): p. 654-659.
51. Arroyo, J.D., et al., *Argonaute2 complexes carry a population of circulating microRNAs independent of vesicles in human plasma.* Proceedings of the National Academy of Sciences of the United States of America, 2011. **108**(12): p. 5003-5008.
52. Vickers, K.C., et al., *MicroRNAs are Transported in Plasma and Delivered to Recipient Cells by High-Density Lipoproteins.* Nature cell biology, 2011. **13**(4): p. 423-433.
53. Small, E.M., Frost, R.J.A., and Olson, E.N., *MicroRNAs Add a New Dimension to Cardiovascular Disease.* Circulation, 2010. **121**(8): p. 1022-1032.
54. Ono, K., Kuwabara, Y., and Han, J., *MicroRNAs and cardiovascular diseases.* FEBS Journal, 2011. **278**(10): p. 1619-1633.
55. Rayner, K.J., et al., *MiR-33 Contributes to the Regulation of Cholesterol Homeostasis.* Science (New York, N.Y.), 2010. **328**(5985): p. 1570-1573.
56. Najafi-Shoushtari, S.H., et al., *MicroRNA-33 and the SREBP Host Genes Cooperate to Control Cholesterol Homeostasis.* Science (New York, N.Y.), 2010. **328**(5985): p. 10.1126/science.1189123.
57. Huang, R.-s., et al., *MicroRNA-155 Silencing Enhances Inflammatory Response and Lipid Uptake in Oxidized Low-Density Lipoprotein-Stimulated Human THP-1 Macrophages.* Journal of Investigative Medicine, 2010. **58**(8): p. 961-967.
58. Cañamares, M.V. et al. Comparative SERS effectiveness of silver nanoparticles prepared by different methods: A study of the enhancement factor and the interfacial properties. J. Colloid Interface Sci 2008 326(1): p. 103-109
59. Dhawan, A. and Sharma, V., *Toxicity assessment of nanomaterial: methods and challenges*. Anal Bioanal Chem, 2010. **398**(2): p. 589–605.
60. Alkilany, A.M. and Murphy, C.J. *Toxicity and cellular uptake of gold nanoparticles: what we have learned so far?* J Nanopart Res. 2010. **12**(7): p. 2313–2333
61. Leopold, N. and Lendl, B., *A New Method for Fast Preparation of Highly Surface-Enhanced Raman Scattering (SERS) Active Silver Colloids at Room Temperature by Reduction of Silver Nitrate with Hydroxylamine Hydrochloride.* The Journal of Physical Chemistry B, 2003. **107**(24): p. 5723-5727.
62. Kimling, J., et al., *Turkevich Method for Gold Nanoparticle Synthesis Revisited.* The Journal of Physical Chemistry B, 2006. **110**(32): p. 15700-15707.
63. Yguerabide, J. and Yguerabide, E.E., *Light-scattering submicroscopic particles as highly fluorescent analogs and their use as tracer labels in clinical and biological applications: I. Theory.* Analytical biochemistry, 1998. **262**(2): p. 137-156.
64. Liu, X., et al., *Extinction coefficient of gold nanoparticles with different sizes and different capping ligands.* Colloids and Surfaces B: Biointerfaces, 2007. **58**(1): p. 3-7.
65. Lee, K.-S. and El-Sayed, M.A., *Gold and Silver Nanoparticles in Sensing and Imaging: Sensitivity of Plasmon Response to Size, Shape, and Metal Composition.* The Journal of Physical Chemistry B, 2006. **110**(39): p. 19220-19225.
66. Alkilany, A.M. and Murphy, C.J., *Toxicity and cellular uptake of gold nanoparticles: what we have learned so far?* Journal of Nanoparticle Research, 2010. **12**(7): p. 2313-2333.
67. Haase, A., et al., *Toxicity of silver nanoparticles in human macrophages: uptake, intracellular distribution and cellular responses.* Journal of Physics: Conference Series, 2011. **304**(1): p. 012030.

68. Graham, D., et al., *Control of enhanced Raman scattering using a DNA-based assembly process of dye-coded nanoparticles.* Nat Nano, 2008. **3**(9): p. 548-551.
69. Fichtlscherer, S., Zeiher, A.M., and Dimmeler, S., *Circulating MicroRNAs: Biomarkers or Mediators of Cardiovascular Diseases?* Arteriosclerosis, Thrombosis, and Vascular Biology, 2011. **31**(11): p. 2383-2390.
70. Kin, K., et al., *Tissue- and Plasma-Specific MicroRNA Signatures for Atherosclerotic Abdominal Aortic Aneurysm.* Journal of the American Heart Association: Cardiovascular and Cerebrovascular Disease, 2012. **1**(5): p. e000745.
71. Vasa-Nicotera, M., et al., *miR-146a is modulated in human endothelial cell with aging.* Atherosclerosis, 2011. **217**(2): p. 326-330.
72. Pamukcu, B., Lip, G.Y.H., and Shantsila, E., *The nuclear factor – kappa B pathway in atherosclerosis: A potential therapeutic target for atherothrombotic vascular disease.* Thrombosis Research, 2011. **128**(2): p. 117-123.
73. Kubota, K., et al., *Improved In Situ Hybridization Efficiency with Locked-Nucleic-Acid-Incorporated DNA Probes.* Applied and Environmental Microbiology, 2006. **72**(8): p. 5311-5317.
74. Thomsen, R., Nielsen, P.S., and Jensen, T.H., *Dramatically improved RNA in situ hybridization signals using LNA-modified probes.* RNA, 2005. **11**(11): p. 1745-1748.
75. Petersen, M. and Wengel, J., *LNA: a versatile tool for therapeutics and genomics.* Trends in Biotechnology, 2003. **21**(2): p. 74-81.
76. Berg JM, Tymoczko JL, and L., S., *Biochemistry*. 5 ed. 2002.
77. Wolfrum, C., et al., *Mechanisms and optimization of in vivo delivery of lipophilic siRNAs.* Nat Biotech, 2007. **25**(10): p. 1149-1157.